Review Article

Bio-mimetic mechanisms of natural hierarchical materials: A review ☆

Qiang Chen[a], Nicola M. Pugno[b,*]

[a]*Laboratory of Biomechanics, School of Biological Science and Medical Engineering, Southeast University, 210096 Nanjing, PR China*
[b]*Department of Civil, Environmental and Mechanical Engineering, University of Trento, 38123 Trento, Italy*

ABSTRACT

Natural selection and evolution develop a huge amount of biological materials in different environments (e.g. lotus in water and *opuntia* in desert). These biological materials possess many inspiring properties, which hint scientists and engineers to find some useful clues to create new materials or update the existing ones. In this review, we highlight some well-studied (e.g. nacre shell) and newly-studied (e.g. turtle shell) natural materials, and summarize their hierarchical structures and mechanisms behind their mechanical properties, from animals to plants. These fascinating mechanisms suggest to researchers to investigate natural materials deeply and broadly, and to design or fabricate new bio-inspired materials to serve our life.

© 2012 Elsevier Ltd. All rights reserved.

Contents

1.   Introduction

Nature, acting as a stealth hand, cultivates and shapes all lives in the planet (Thompson, 1945). It provides a huge amount of biological materials with different functions, such as, abalone nacre (Curry, 1977), crab exoskeleton (Chen et al., 2008a,2008b,2008c), turtle shell (Rhee et al., 2009), armadillo shell (Chen et al., 2011), and gecko feet (Autumn et al., 2000). Several decades ago, most of these biological materials were explored only by biologists. However, since Material Science and Engineering (MSE), a vibrant discipline, emerged in the 1950s, biological materials have been being added to its interest from the 1990s and drawn much attention due to their fascinating multi-functionality (self-organization, self-assembling, self-healing, self-cleaning, etc., Meyers et al., 2008a,2008b). For instance, on the one hand, from the point of view of mechanics, natural materials usually exhibit many interesting properties, e.g. light-weight, high-toughness (Ritchie et al., 2009), mechanical-efficiency (Wegst and Ashby, 2004), flexible-switch attaching and detaching (Tian et al., 2006), and self-cleaning properties (Cheng et al., 2006; Lepore and Pugno, 2011), etc. In particular, nacre shell, with brittle bio-mineralized tablets and a small percent of organic matrix, has excellent mechanical properties (Jackson et al., 1988; Schäffer et al., 1997; Kamat et al., 2000; Lin et al., 2006; Espinosa et al., 2011), and its toughness is approximately 3000 times greater than that of a single crystal (Song et al., 2003). On the other hand, from the point of view of other physical properties, Bejan (2000) proposed a law for the occurrence of shape and structure configurations; after that, employing the law in minimizing the body heat loss and blood pumping power, he predicted the proportionality between metabolic rate and body mass to the power 3/4 (West et al., 1997; Bejan, 2001,2005; Guiot et al., 2006, 2007; Brianza et al., 2007; Pugno et al., 2008a; Delsanto et al., 2008,2009).

Inspired by these interesting phenomena, researchers start to reveal their components and find that even though natural materials, e.g. bone, show various abilities due to their different ambient environments (Srinivasan et al., 1991), they often possess two major constituents: biopolymer and bio-mineral,

which are made of several fundamental elements, primarily C, N, Ca, H, O, Si (Chen et al., 2008a, 2008b, 2008c; Meyers et al., 2008a,2008b); the two constituents are often quite weak compared with their final smart "products" (Fratzl and Weinkamer, 2007). Then, questions rise: How nature can build so strong/ tough materials or structures with such weak constituents? Why natural materials have a variety of structures and functions, e.g. difference between bones and tendons, though they have same constituents? What is the structure–function relationship behind these properties? Although Wegst and Ashby (2004) have established elevation indices and presented them as materials property charts/Ashby map for natural materials, how nature develops the mechanical efficiency of natural materials is still unknown. With these doubts, material scientists and engineers are devoting themselves to dig the principles and mechanisms out (Smith et al., 1999; Autumn and Peattie, 2002; Qin et al., 2009; Nova et al., 2010) and try to pave a way to fabricate bio-mimetic materials. In this regard, Fratzl (2007) provided a guideline to realize the process, which is divided into three steps: (1) Elucidating structure–function relationships of biological materials; (2) extracting the physical/chemical principles of the relationships; (3) developing manufacturing technologies to synthesize bio-inspired materials. The first step starts with experimental observations of natural materials, which give us an intuitive correlation between structure and function; then, basing on these experimental images and data, the quantitative relationships or principles between structures and functions are extracted; finally, the new bio-inspired materials are designed. In line with these steps, to date, an abundant of experimental observations and developed theories on different natural materials are obtained, such as recent developments on gecko foot (Autumn et al., 2006a,2006b; Pugno and Lepore, 2008a,2008b; Varenberg et al., 2010), nacre shell (Espinosa et al., 2011), Armadillo armor (Chen et al., 2011). These studies show that hierarchical structures at several length scales, from nano- to macro-scale, determine the functions of natural materials, and the structure at each hierarchical level is optimized by Nature. Many biomimetic materials have already been synthesized, such as, gecko tape inspired by *Gecko* (Geim et al., 2003) and

self-repairing slippery surfaces by *Nepenthes* (Wong et al., 2012). Several works summarized the contributions from the stand of the structure–function relationship. The earlier work can be traced to the review by Srinivasan et al. (1991); in this work, they characterized the natural materials from the features of the multi-functionality, hierarchical structures, adaptability, and reviewed the structural and mechanical properties of natural materials—wood, insect cuticle, bone and mollusk. Later, Lakes (1993) reviewed mechanical properties of several typical materials with structural hierarchy, which included man-made structures, e.g. the Eiffel tower, natural materials, e.g. tendon and hierarchical cellular solids. Recently, considering the functional adaptation (in particular, mechanics) of structures at all levels of hierarchy, Fratzl and Weinkamer (2007) summarized work on revealing basic principles, which are employed by Nature to design natural cellular materials (bone, wood, and glass sponge skeletons) and an elastomer (tendon); Buehler et al. (2008) focused on protein materials (e.g. spider silk) and employed multi-scale approaches (especially, large-scale atomistic simulations) to study and understand dynamic and fracture mechanisms that happen at nano- or meso-scale; furthermore, starting with the basic building blocks, i.e. biominerals, proteins and polysaccharide, Meyers et al. (2008a,2008b) illustrated systematically the growth mechanism and hierarchical structures of the four types of natural materials, which are categorized according to Wegst and Ashby (2004); Espinosa et al. (2009) described the microstructure and mechanics of nacre and bone, and reviewed the fabrication of nacre-inspired artificial and related materials; Curry (2010) reviewed some less familiar bony tissues, e.g. deer's antler; Bhushan and Jung (2011), addressing the properties of natural and bio-mimetic surfaces, reviewed the latest achievements and developments; Jagota and Hui (2011) systematically reviewed recently developed bio-inspired materials and discussed the surface mechanical properties—adhesion, friction, and compliance and discussed the relationship between structural parameters and mechanical behaviors.

In this review, we focus ourselves on several selected natural materials and summarize their bio-mimetic mechanisms, which are extracted from a huge amount of literature. Nacre shell, gecko foot, mussel and spider silk are well-known natural materials and have been studied for a very long time; here, we overview some classical and recent literature to discuss respectively the toughening mechanisms for nacre shell and spider silk, and adhesion mechanism for gecko foot and mussel. As for the exoskeleton of lobster or crab, armadillo shell, turtle carapace, diatoms and plant stem, new developments on these fields are reviewed; the light-weight but mechanical-efficiency cellular structures are unveiled and the biomechanical properties are illustrated. This paper does not have the aim to present a complete review but to discuss some new and important results.

2. Nacre/seashell

Nacre shells (Fig. 1) are comprised of aragonite platelets and organic matrices, and exhibit two-level crossed lamellar micro-architectures (Pugno, 2006); aragonite platelets (about 5–8 μm in diameter and about 0.5 μm in thickness) act as "brick" with weight fraction 95–97% and organic matrices (about 20–30 nm thick) as "mortar" with weight fraction 3–5% (Curry, 1977; Stempflé et al., 2010). The function of the platelets is increasing the structural stiffness and hardness, whereas, the function of proteins between layers is controlling the nucleation and growth of the inorganic phases in a bio-mineralization process of these structures (Kaplan, 1998; Rousseau et al., 2005,2009). As for the observed high toughness, it is well-known that the key mechanism is due to a sophisticated interfacial architecture and produced by the sliding of inter-platelets (Rim et al., 2011), which can dissipate a considerable amount of energy; addressing this problem, we here categorized the toughening mechanisms into five groups: (1) interlocking of nano-asperities, (2) weak organic interfaces, (3) inter-lamellar mineral bridges, (4) plastic deformation of individual tile, and (5) multiple cracking and large-scale crack bridging.

2.1. Toughening mechanisms

2.1.1. Interlocking of nano-asperities
The existence of nano-asperities and sliding between them can form multiple dilation bands at the inter-lamellar boundaries (Fig. 2a); on these boundaries, the stress is redistributed and thus, the deformation shows an inelastic behavior (Wang et al., 2001; Li, 2007). In the sliding process, the interface produces elastic friction and makes nano-grains (or waviness) on the surfaces of platelets interlock (Barthelat et al., 2007; Fig. 2b), which can induce the anisotropy under loading conditions and large energy absorption capacity; plus, the
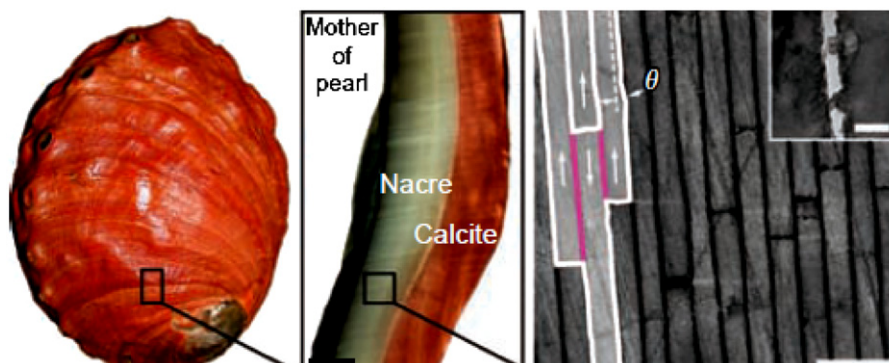
Fig. 1 – Hierarchical and brick-mortar structure of Abalone nacre (Espinosa et al., 2011).
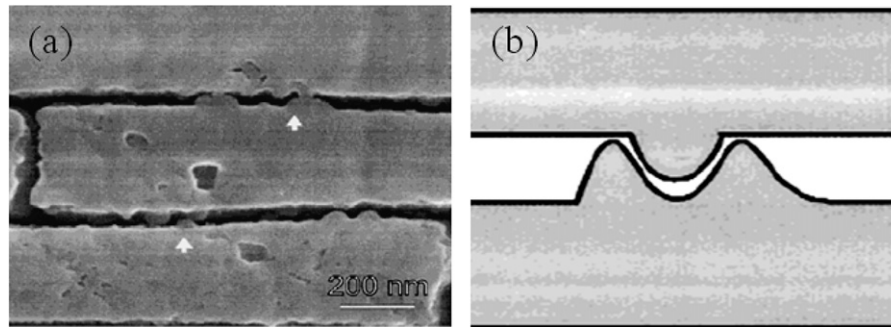
Fig. 2 – (a) SEM image of nanoasperities on the surface of platelets; (b) schematic of the interlocking between nanoasperities (Wang et al., 2001).
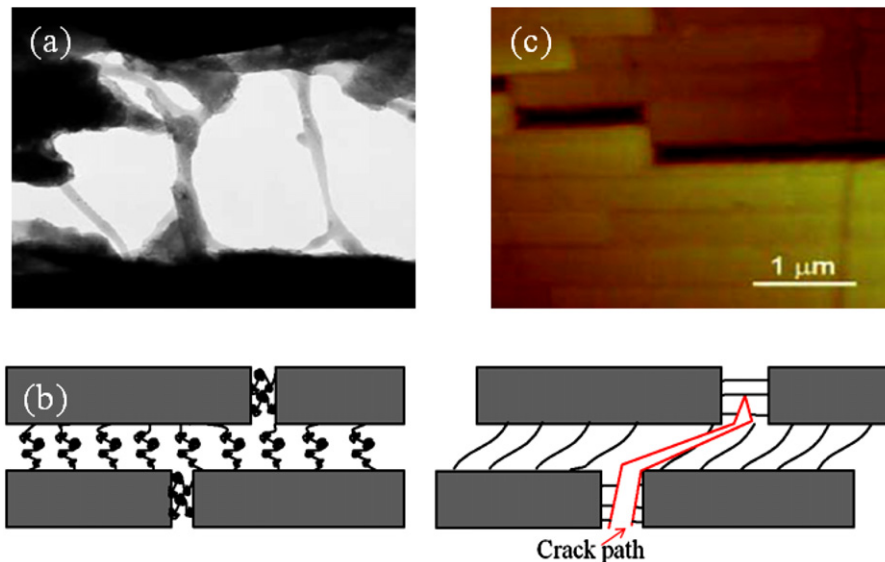
Fig. 3 – (a) SEM image of adhesive ligaments between platelets (Smith et al., 1999); (b) schematic sliding between platelets and crack deflection; (c) SEM image of crack deflection (Li, 2007).

interlocking effect provides a high resistance to crack propagation, tolerance to local imperfects and establishes the stress level needed to attain the inelastic strain (i.e. strain hardening), which is considered as a principal toughening mechanism (Espinosa et al., 2011); moreover, the interlocking interface can realize the overall structural integrity by topologizing the fragmental aragonite platelets (Estrin et al., 2010).

2.1.2. Weak organic interface
In this toughening mechanism, the organic matrix is considered as an adhesive to glue the platelets together (Fig. 3a). When shells are tensioned, the deformation is mainly caused by the interfacial shear and the high toughness is attributed to the unfolded loops/domains of organic proteins (Smith et al., 1999; Fig. 3b), which was treated as a coiled-spring model and investigated further by Xu and Li (2011). The weak interfacial design permits stress redistribution around the strain-concentration sites and leads to crack path deflection due to the stress shielding (Clegg et al., 1990; Launey and Ritchie, 2009; Fig. 3c). Ritchie (1988) analyzed several toughening mechanisms, and for this phenomenon, the material

toughness was expressed as $K_I = K_{tip} + K_s$, where, K_I is the applied stress intensity factor, K_{tip} is the local near-tip stress intensity factor, and K_s is the stress intensity factor due to shielding. We can see that increasing K_s reduces K_{tip} at constant K_I and thus the material toughness is enhanced.

2.1.3. Inter-lamellar mineral bridges
Different from the above cases, from Fig. 4a we can see that there are pores in the sheet of organic matrix layers with 20–30 nm radius; these pores allow platelets to grow mineral bridges with 5–50 nm in size (Fig. 4b) through them, connecting adjacent aragonite platelets (Schäffer et al., 1997; Song et al., 2003; Meyers et al., 2008a,2008b). When an external force is imposed, the mineral bridges and the organic matrices share the load; at the beginning, the mechanical behavior is nearly linear-elastic; as the force increases, the mineral bridges break; the friction between aragonite platelets, which causes the strain hardening energy and unfolding of the organic protein, emerge to resist the sliding movement. Therefore, in this case, the mechanism could be regarded as a coaction of the above mechanisms after failure of the mineral bridges.

2.1.4.   Plastic deformation of individual tile

The previous three mechanisms have one thing in common, that is, the interfacial architecture and sliding. However, Li et al. (2004) observed that not only the sliding movement between aragonite platelets is the cause of the plastic deformation of shells but also aragonite platelets themselves are ductile. Besides, the model basing on stiff aragonite platelets was not able to explain the particular mechanical behavior, which occurred under dynamic solicitations (Stempflé and Pantalé, 2007); these authors found that the plasticity of an individual platelet was due to the intra-crystalline matrix (Fig. 5b), the elastic modulus of which was two times lower than that of the inter-crystalline phase; so, they concluded that the intra-crystalline matrix governs the plastic deformation of the single platelet and therefore the overall deformation of the nacre (Stempflé et al., 2010). Also, the fracture of individual platelet was investigated by Lin and Meyers (2009).

2.1.5.   Multiple cracking and large-scale crack bridging

As we know, high toughness usually is achieved during crack propagation (R-curve behavior), and materials can absorb more fracture energy (Launey and Ritchie, 2009). Here, different from abalone shell, *Strombus gigas* conch shell has a spiral configuration and a lower strength than that of abalone shell, due to their different microstructures (Lin et al., 2006); for the conch shell, two energy-dissipating mechanisms are invoked, i.e. multiple micro-cracking in the outer layer at low loading levels and crack bridging in the middle one at high loading levels (Kamat et al., 2000; Fig. 6). Under low loads, the external work is absorbed by the propagation of the micro-cracks in the outer layer, while the middle layer prevents the crack propagation (intrinsic toughening mechanism); as the load increases, the energy absorption saturates in the outer layer and the cracks reach the middle one and grow while the crack bridging developed in the outer layer restrains the crack growth in the middle one (extrinsic toughening mechanism).
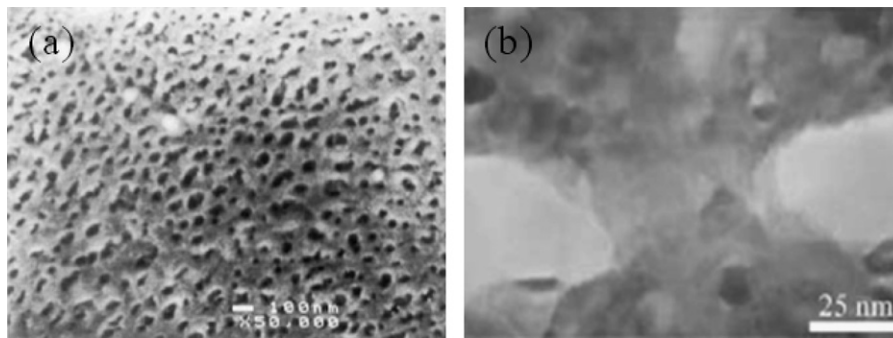
Fig. 4 – (a) SEM image of interlamellar organic matrix layers with holes (Schäffer et al., 1997); (b) TEM image of mineral bridge between adjacent platelets (Song et al., 2003).
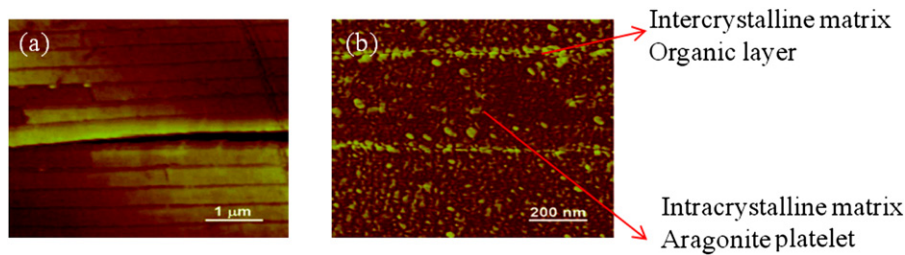
Fig. 5 – (a) Cross-section of nacre; (b) intercrystallinne matrix and intracrystalline matrix (Li et al., 2004).
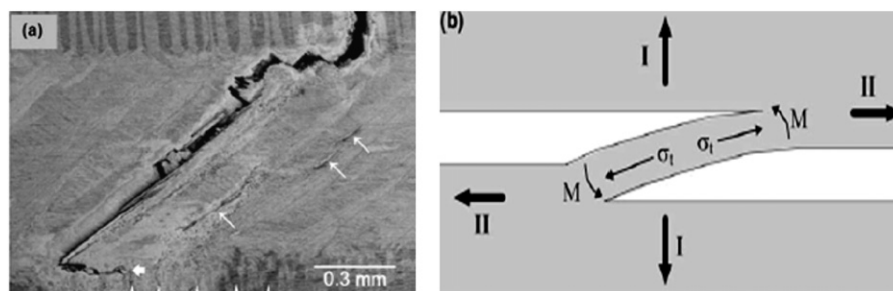
Fig. 6 – (a) Ligament bridging a delamination between the middle and outer layers of the shell (Kamat et al., 2004); (b) model for crack bridging by misaligned fibers (Cox and Marshall, 1994).

The interacting process leads to the high toughness. Indeed the organic phase also plays an important role in the process (Kamat et al., 2004).

2.2.   Theoretical models

Basing on the aforementioned mechanisms, some models and principles were extracted to build the structure–function relationship for future bio-inspired material design. A simple physical model of nacre (platelet-reinforced composites) was built by Jackson and Vincent (1989); Young's modulus was predicted by the rule of mixture, incorporating shear-lag models, and the tensile strength determined by the interfacial shear was predicted by pull-out failure mode; the two predictions agreed with the experimental data very well, however, the model failed to mimic the fracture toughness. Lin et al. (2006) employed the classical Weibull statistic strength theory to compare the mechanical strengths of *Strombus Giga*, *Tridacna Gigas*, and *Haliotis Rufescens* seashells, and found $\sigma_{Tridacna} < \sigma_{strombus} < \sigma_{Haliotis}$. Tang et al. (2007) proposed an elasto-visco-plastic interface model with a constitutive relationship to understand the strengthening mechanism, and the numerical simulations showed a hardening deformation, which was consistent with the previous experimental results. Recently, Rim et al. (2011) have developed a composite-computational model to investigate the influences of geometrical parameters and intrinsic material properties of constituents, incorporating the key morphological features; the results showed that an optimal geometry could increase the toughness by 70 times.

Different from others, Jäger and Fratzl (2000) first presented and discussed a mechanical model (or Jäger–Fratzl model) of mineralized fibrils, where mineral platelets are arranged in parallel and staggered arrays. Following this model, Gao et al. (2003) reported that the strength and toughness of natural composites materials, including nacre and bone, are insensitive to flaws at nano-scale, which is called principle of flaw-tolerance; this principle plays an important role in determining the materials' high strength and toughness. Sen and Buehler (2011) explained that this principle and the related high toughness (*R*-curve behavior) is due to the incorporation of the hierarchy in the design; by studying a silica hierarchical structure, they found that the insensitive size can approach hundreds of micrometers. This principle is very useful to design the next generation of nanomaterials. Ji (2008) incorporated the tension-shear chain (Ji and Gao, 2004; Fig. 7a) into the Dugdale model (Dugdale, 1960) to investigate the hybrid interfacial strength and estimate the fracture energy; in this work, they also included viscoelastic properties of the protein-mineral nanostructure and showed that the toughness of this biocomposite can be further enhanced by the viscoelastic properties of protein. Moreover, combining this model (Fig. 7b) with a homogenization theory, Bertoldi et al. (2008) proposed a micromechanical model to study the macro-mechanical behavior of nacre, and the analytical results showed that nacre was orthotropic and had different Young's modulus when compressed and tensioned, consistent with existing experimental and numerical data. Recently, a new-developed micromechanical model (Begley et al., 2012), so-called "brick-mortar model", which is derived from the tension shear chain model, is analyzed in order to calculate the effective

properties of the bioinspired brick and mortar composite (Wilbrink et al., 2010); employing this model they studied the competition between elastic modulus, strength and work-to-failure by considering the failure transition between brick rupture and rupture of the interfaces.

Therefore, either from experimental observations or theoretical models, both the interface and platelet contributions to the toughness of the shell or shell-like structures are significant and thus represent a robust bio-inspired principle.

3.   Gecko feet

Gecko feet attract people's attention for a long time, because of their capacity running on vertical walls freely. Under SEM, gecko foot exhibits a typical hierarchical structure (Fig. 8) and it contains about 0.5 million setae (Autumn et al., 2000), of which distribution density is 5000 setae/mm². If one gecko foot can produce 10 N adhesive force, which is much greater than gecko's body-weight, then, each seta will carries 20 μN. This is why the gecko can stay on the vertical wall without slipping and explains the excellent adhesive ability. However, because geckos need to move fast on the wall when preying or escaping, they must switch easily from the attaching state. Therefore, in order to design gecko-pad-inspired materials, the attaching and detaching phenomena have driven many scientists to reveal the mechanisms, which in essence are problems of surface contact and fiber adhesion. In the following subsections, we will discuss the related mechanisms.

3.1.   Attaching/detaching mechanisms

3.1.1.   Attaching mechanisms
In the dry environment, employing a two-dimensional micro-electro-mechanical systems force sensor, an experiment directly measuring a single setal force was performed (Autumn et al., 2000,2002), and the results supported the assumption that
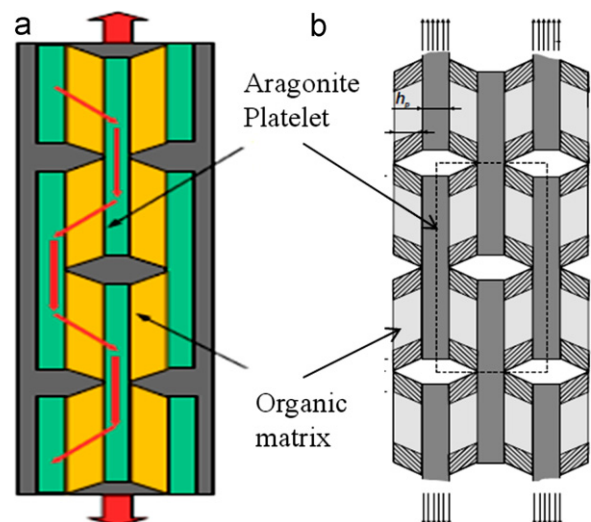
Fig. 7 – Tension-shear chain model (Ji and Gao, 2004; Bertoldi et al., 2008).
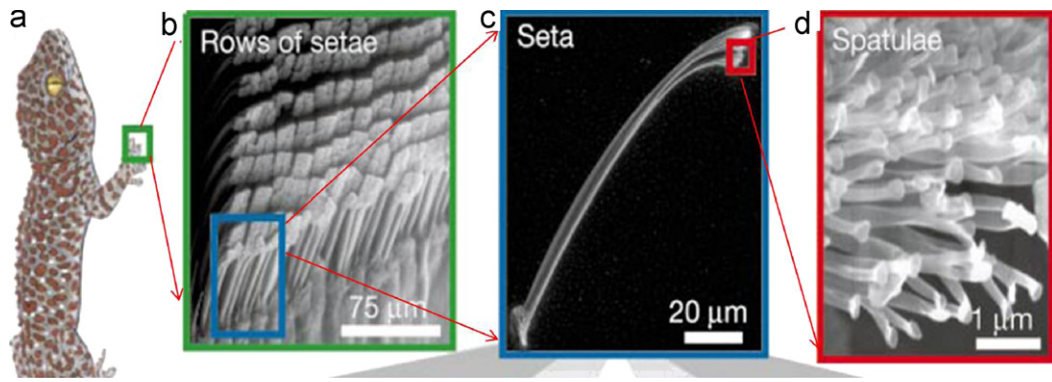
Fig. 8 – Hierarchical structure of a gecko foot. (a) Gecko; (b) seta row; (c) single seta; (d) spatulae (Autumn et al., 2000).
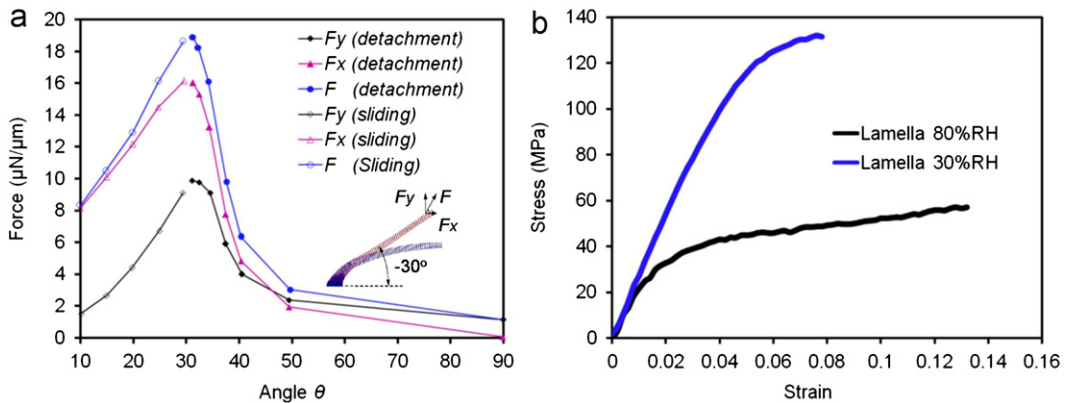
Fig. 9 – Analysis of the pull-off force of a single seta as a function of the pulling orientation (Gao et al., 2005); (b) tensile stress–strain relationship of gecko lamella at 30% and 80% RH (Prowse et al., 2011).

the intermolecular force—van der Waals—played a vital role in the single seta attachment, which is merely a matter of the tip size and shape, but reported a weak dependence on surface chemistry and rejected the influence of high surface polarity (e.g. capillary adhesion); moreover, due to the unique uncurling and peeling behaviors (Russell, 1975), macroscopic orientation and preloading of the seta result in higher attachment force, 600-fold above that of frictional measurements, and this is why they rejected the two proposed mechanisms, i.e. suction and friction. Meanwhile, a large difference between the adhesive force of the single seta and that of measured in the whole gecko under a small normal preload was discovered. Addressing this difference, later, Autumn and Peattie (2002) proposed an integrated approach, from molecules to the entire gecko, by correlating the adhesion energy between a gecko seta and a surface to the water droplet contact angle; this revealed that a nearly 30° peeling angle results in the easiest detachment. Yao and Gao (2006) obtained the same result by utilizing fracture mechanics and numerical simulations as shown in Fig. 9a. In the wet environment, Huber et al. (2005) found an evidence of humidity contributions of the adhesion force at the spatula level, which is the lowest level of the gecko-foot hierarchical structure; this finding suggested a role of the capillary force, produced by the monolayer water adsorption between spatula and substrate. Recently, Prowse et al. (2011) also reported that increasing humidity improves the adhesion and friction force, and produces a significant influence on the mechanical properties

(elasticity, strength, fracture and dynamics) of setae and setal lamina, see Fig. 9b; Fig. 9b shows that as humidity increases Young's modulus of lamella decreases, whereas the failure strain increases. Regarding the opposite conclusions on the influence of the capillary effect made by Autumn et al. (2002) and Huber et al. (2005), a possible explanation is that the gecko seta is stiff in dry conditions but soft in wet conditions; moreover, the latter condition can improve the fracture energy apart from the contribution of capillary.

3.1.2. Detaching mechanism
Regarding the detaching mechanisms, two known mechanisms are extracted, namely, at the micro-scale, the seta detaches when the seta shaft (Fig. 10a) reaches a critical angle with the substrate; at the macro-scale, geckos hyperextend their toes. However, because the peeling angle raises a question when gecko is inverted on ceilings, that is to say, the gecko must maintain the adhesive state under its body mass, which causes the increase of the peeling angle, Autumn et al. (2006a,2006b) proposed a frictional-based adhesive mechanism for this peculiar case and demonstrated that adhesion depends directly on shear force instead of the peeling angle; the relationship between adhesion and shear force is consistent with a critical angle of release in live geckoes. Different from the rejection of the tape-peeling hypothesis (Autumn et al., 2006a,2006b), Pugno et al. (Varenberg et al., 2010; Pantano et al., 2011) considered
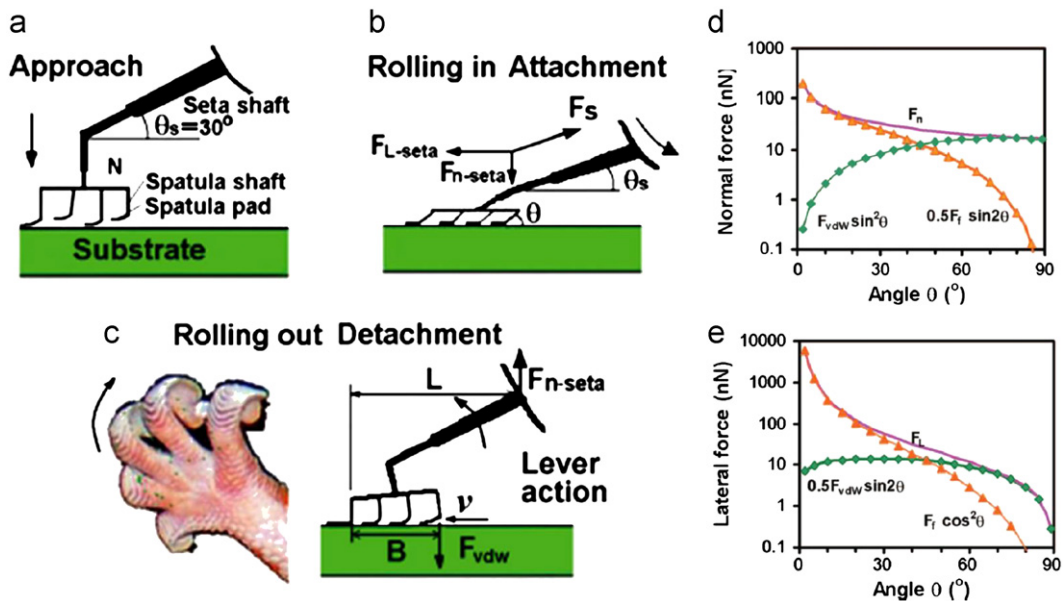
Fig. 10 – Schematic of mechanisms of attachment and detachment. (a) A single seta; (b) rolling down for attachment; (c) rolling up for detachment; (d) total normal adhesion force F_n and (e) total lateral force F_L of a single spatula, and the contributions from F_{vdW} and F_f to them (Tian et al., 2006).

the detaching problem as a peeling process, which is regarded as the governing mechanism at all different hierarchical levels (Pugno, 2011), and they employed the Kendall model to investigate the influences of peeling angle, thickness gradient and shape of the spatula-like structures on the peeling force. Addressing the different results, Tian et al. (2006) theoretically analyzed the interaction between the spatula and substrate by incorporating both van der Waals (or adhesion force) and friction force; rolling down and gripping toes inward produced a small contact angle and made gecko able to obtain a strong attachment (Fig. 10b); by contrast, rolling toes up and back produced a low adhesion-to-friction ratio, helping the perpendicular peeling off of the spatula from the substrate (Fig. 10c); from Fig. 10d, e, we can see that the van der Waals and friction force contributions to the resultant normal and lateral forces can be calculated by $F_n = 0.5F_f\sin2\theta + F_{vdW}\sin^2\theta$ and $F_L = F_f\cos^2\theta + 0.5F_{vdW}\sin2\theta$ respectively; in particular, when $\theta < 45°$, the friction force makes a greater contribution to the normal and shear forces; otherwise, i.e., for $\theta > 45°$, van der Waals force prevails. This explains the different mechanisms for different peeling angles. Besides, according to the peeling model, an anisotropic elastic solid exhibits a strongly anisotropic adhesion strength when sticking on a rough surface (Yao and Gao, 2006).

3.2. Optimization problems

Gao et al. (2004) applied the principle of flaw tolerance (Gao et al., 2003) to the nanostructures of biological systems; they showed that spatula geometry, the finest structure in the structure of gecko foot, had an influence in determining the adhesion strength (Fig. 11) and the influence of the tip shape in fibrillar structures on the adhesive optimization (Gao and Yao, 2004); the result displayed that when the diameter reduced to 100 nm, the variation in shape produced weaker influences. The flaw tolerant hypothesis was fully verified by an atomistic and continuum study at small scales (Buehler et al., 2006). Moreover, the authors studied the adhesive properties with a hierarchical approach (Chen et al., 2008a,2008b,2008c; Yao and Gao, 2006) and showed that the size of each hierarchical level was optimized as well.

Besides, Persson (2003) and Persson and Gorb (2003) studied the mechanism of the adhesion in biological system (e.g. gecko and fly). They discovered that the small effective elastic modulus of the setae array was a basic influence on the adhesion on a hard but rough surface, and reported that the setae array had a large contact angle and exhibited a self-cleaning function; the self-cleaning was first analyzed, with water contact angle, by Autumn and Peattie (2002) and later verified by Hansen and Autumn (2005). Other authors (Pugno and Lepore, 2008a,2008b; Pugno et al., 2011; Lepore et al., 2008,2012a) investigated the adhesive time of male/female geckos on different rough surfaces and found that the time to failure obeys a Weibull statistical distribution and optimal angle for the maximal adhesion in living tokay geckos. Autumn et al. (2006a,2006b) studied the dynamics of geckos running on a vertical wall and found that different legs had different functions, to make gecko move faster.

4.   Mussel

In the underwater environment, the gecko feet lose their adhesive capacity (Lee et al., 2007). Different from the gecko
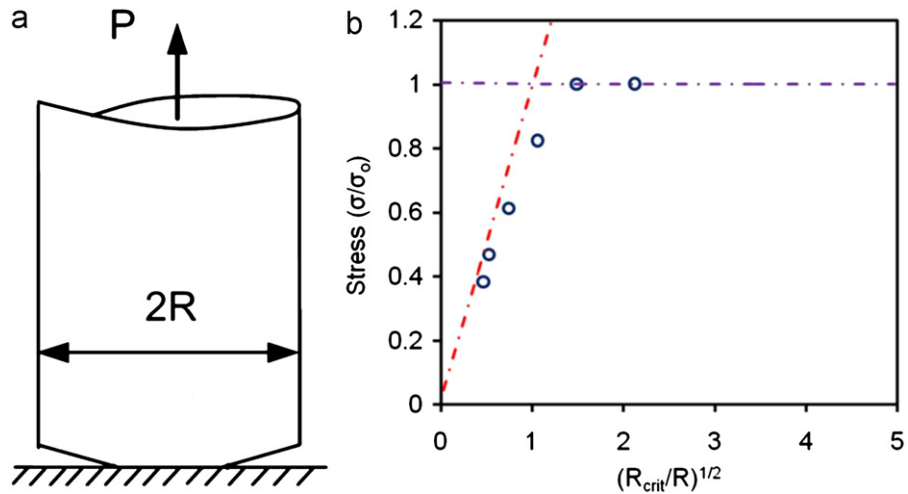
Fig. 11 – Flaw tolerant adhesion: (a) schematic of the spatula; (b) atomistic simulation results . Data from (Buehler et al., 2006).
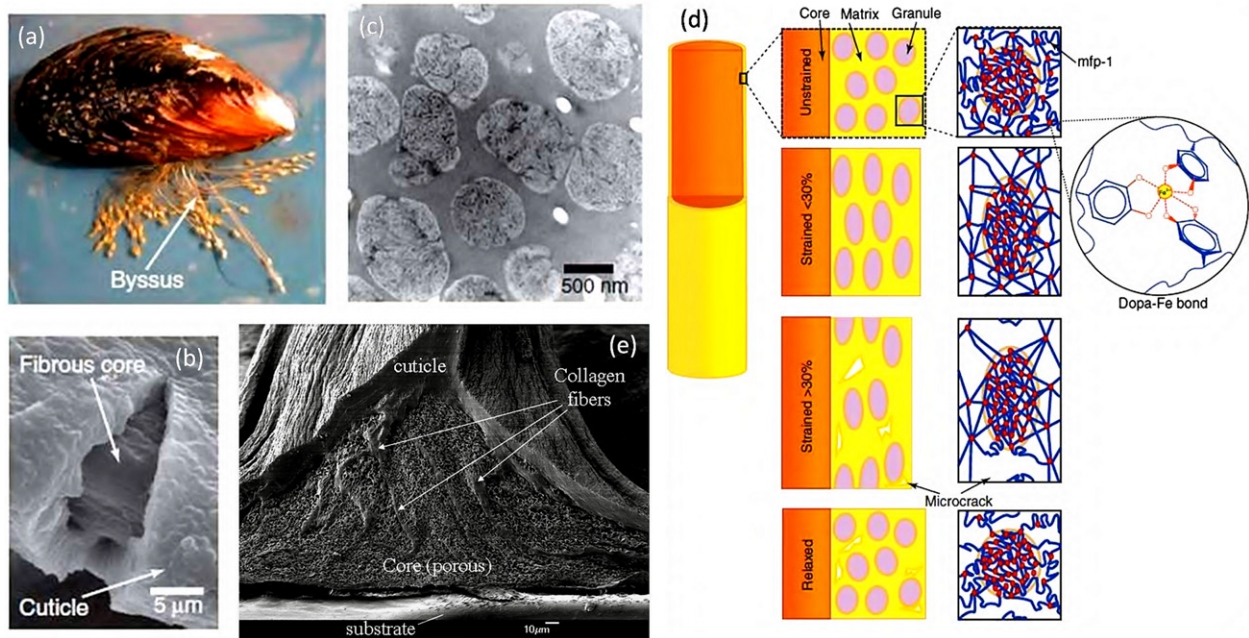
Fig. 12 – (a) Numerous extensible, shock absorbing byssal threads (the white arrow); (b) byssal thread microstructure-cuticle and core; (c) granular structure in thread cuticle; (d) hexadentate mononuclear tris DOPA-Fe coordination complex cross-link MFP-1; (e) hierarchical model illustrating the role of DOPA-Fe complexes in the byssus cuticle (Harrington et al., 2010); (f) SEM image of the adhesive plaque core (Waite et al., 2005).

feet, the underwater mussel can bond to rocks through its adhesive plaques at the end of byssal threads (Harrington et al., 2010; Fig. 12a; Shafiq et al., 2012), which take several minutes to be made, and the interfacial and cohesive mechanical strength and durability can be both improved through a single organic functionality with a versatile chemical reactivity tuned by sea water triggers. The adhesive feature can also be found in other underwater creatures, such as sea cucumber. This is very interesting for designing underwater adhesive devices, thus, we will focus on the structure and its excellent adhesive behavior in this section.

4.1.   Structure properties of byssal thread

First, we examine a single thread, its structure is shown in Fig. 12b; we can see that it is constructed by two components: one is the cuticle, with a $\sim$5 μm thickness, and the other one is the fibrous core; the former exhibits a hardness four- to five-fold higher than the latter while maintain a breaking strain as high as 100%. The cuticle has a microstructure with granular proteins (Fig. 12c) embedded into a matrix and is the granular proteins that hinder the crack propagation and allow to reach a great toughness, similarly to the toughening mechanism by coarse
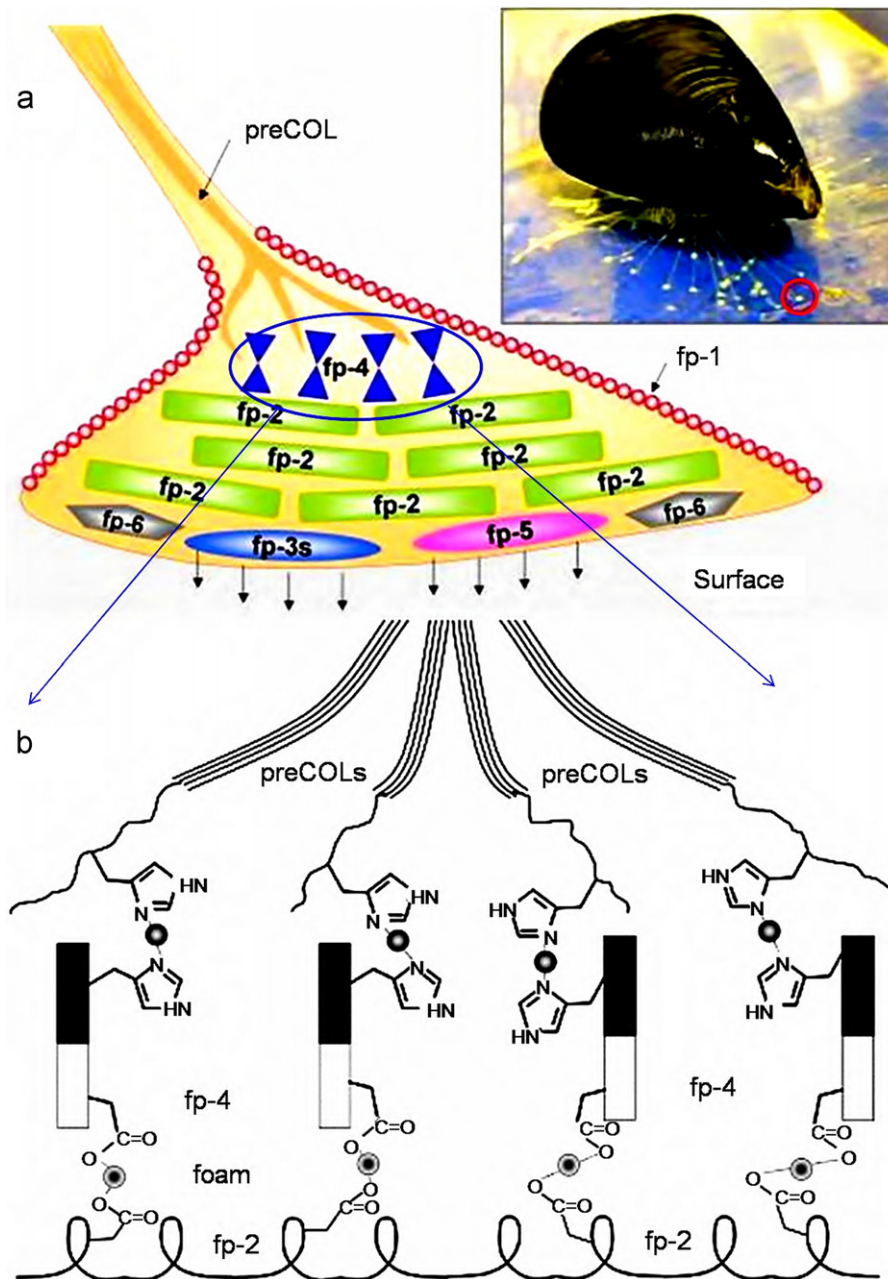
Fig. 13 – (a) Byssal plaque proteins of Mytilus. Inset is a mussel attached to a sheet of mica (Hwang et al., 2010); (b) model of fp-4's role in the joint of his-rich domains of preCOLs and other binding proteins in the foam (Zhao and Waite, 2006).

aggregates in concrete. Considering the excellent structural and mechanical properties of the covered cuticle, a basic hierarchical model is presented in Fig. 12d. It shows that the metal cation ($Fe3+$) plays a vital role in forming a DOPA-Fe complex and further the cross-linking polymers result in stronger materials (Pugno, 2010); besides, the complex provides significant interactions for the integrity of cuticles deformed under tension (Holten-Andersen et al., 2009). As for the fibrous core, it is a open-cell structural foam with treeroot-like collagen fibers going through (Waite et al., 2005; Fig. 12e); moreover, pore size grows large from the plaque to the neighbor of the cuticle, which forms a porosity gradient. This architecture is maybe due to the requirement of the interfacial strength, which results in a hard matter at the bottom of the plaque, and the pores in the center,

or at the top of the plaque, can resist crack propagation. This structural feature can also be found in other biological materials, e.g. the lobster, as we will see in the following sections.

4.2. Plaque adhesion mechanism

We have mentioned that the adhesion plaques of byssal threads contact with solid surfaces, and form a strong bonding; in this case, the protein molecular requirements must be satisfied, see Fig. 13. In Fig. 13a, the adhesive plaque contains the mussel foot protein-1 (MFP-1), MFP-2, MFP-3, MFP-4, MFP-5 and MFP-6. These proteins contain more or less DOPA, which is very important in the adhesive process. Recently, the mechanics of the DOPA was studied by
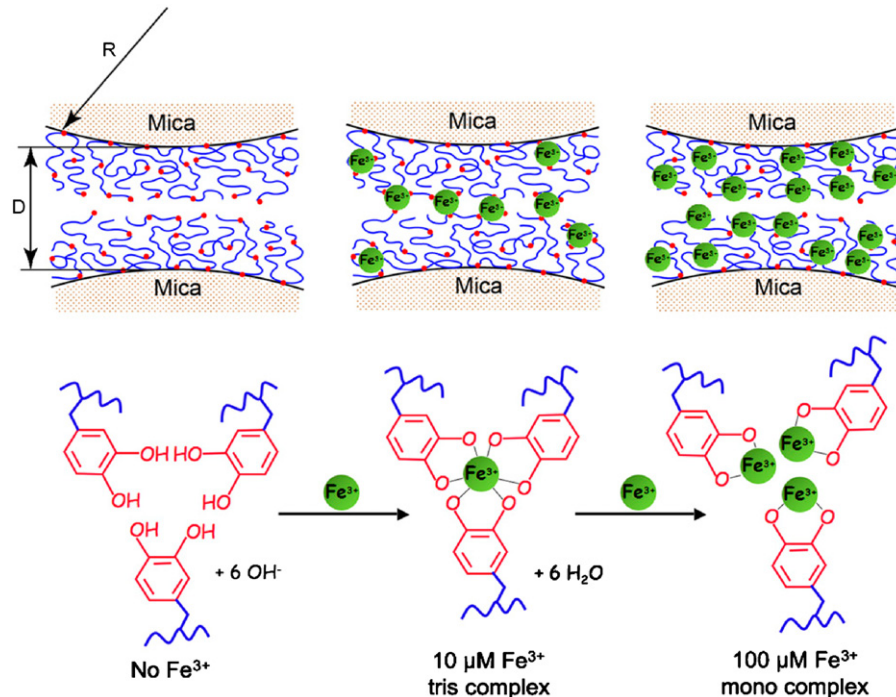
Fig. 14 – Symmetric deposition of mfp-1 on opposing mica surfaces (Zeng et al., 2010).

molecular dynamics simulations (Qin and Buehler, 2011, 2012), revealing that the mechanism of such strong adhesion is governed by a pair of hydrogen bonds between substrate and DOPA, which has a strong affinity to a silica surface.

MFP-1 is deposited as a protective coating and can adhere well on mica (the left one in Fig. 14), which functions similarly as that presented in the cuticle (Lin et al., 2007; Fig. 12e), and with a moderate Fe^{+3} concentration, close to the ionic strength in seawater; two MFP-1 films are bridged (the middle one in Fig. 14) with a distance D and Fe^{+3}-mediated bridging is reversible as the Fe^{+3} concentration increases (Zeng et al., 2010; Fig. 14, right).

MFP-2 is rich in the plaque, joins the thread to the plaque at the top and binds to the proteins (MFP-3 and/or MFP-5) that connect the footprint of the plaque to foreign surfaces at the bottom; the protein–protein interaction between MFP-2 and MFP-5 is strong and reversible in the presence of Fe^{+3} and Ca^{+3}, which also controls the bonds between MFP-2s. Hwang et al. (2010) assumed that MFP-3 may completely displace MFP-2 to become the only adhesive protein; at the same time, they also presumed that binding to MFP-3 is mediated by some other plaque proteins.

MFP-3 and MFP-5 are known to be strongly adhesive (Liu et al., 2007) due to their DOPA-rich interfacial adhesive protein, and these two kinds of proteins play an important role in the adhesion on substrates. In contrast to MFP-3 and MFP-5, MFP-6 contains less DOPA, so it is not so adhesive, but it may provide a cohesive link between the surface-coupling DOPA-rich proteins and the bulk of the plaque proteins. MFP-4 is a matrix protein between collagen fibers and foam-like adhesive plaques, and further acts as a macromolecular bi-functional linker by using metal ions to couple its own His-rich domains to the His-rich termini of the preCOLs (Zhao and Waite, 2006; Fig. 13b).

Besides, the seawater pH-value also produces a strong influence in the protein activity (Holten-Andersen et al., 2011), such as $pH > 7$ form Fe^{3+}-catechol (included in DOPA) cross-links, which are related to the protein interactions; the shear effect between the plaque and the surface can significantly increase the adhesion, and the high adhesion and friction is achieved at a peeling angle around $20°$. Finally, the work by Lin et al. (2007) indicated that the adhesion on mica is produced by weak physical interactions rather than chemical bonding, and that the strong adhesion forces of plaques arise as a consequence of their geometry (e.g., their inability to be peeled off) rather than a high intrinsic surface or adhesion energy. These results are similar as that of gecko feet, for example, the peeling angle for gecko-feet spatula is around $30°$, but with different peeling directions, the angle varies from $15°$ under shear force to $50°$ under normal force; moreover, both gecko and mussel adhesion are only the result of the geometries of their spatula tip or plaque.

5. Spider silk

Spider silks have different functions, such as protective housing and traps (Foelix, 1996). However, the most interesting webs are able to capture high velocity insects when flying (Vollrath, 2000), possess a high damping capacity which is considered as a result of evolution and dissipate kinetic energy caused by large, energetically valuable preys (Kelly et al., 2011). This is attributed to their high strength, toughness, extensionality and torsional qualities (Emile et al., 2006; Lepore et al., 2012b; Giesa et al., 2011). In particular, the orb-
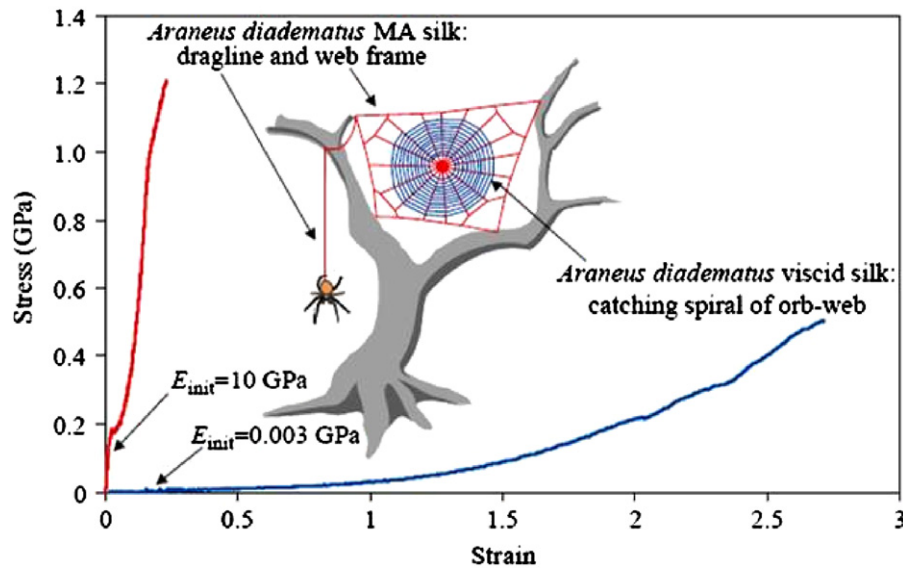
Fig. 15 – Stress–strain relationships of two types of silks in orb-weaving spider web (Gosline et al., 1999).

weaving web are widely studied; the web is constructed by web frame and dragline, excreted by the major ampullate (MA) gland, and viscid silk, produced by the flagelliform (FL) gland, which have different properties (Fig. 15; Gosline et al., 1999). Fig. 15 shows that the dragline silk or web frame is stiffer, but viscid silk is tougher. This is probably because the grade of mechanical properties is more suitable for absorbing the impact energy caused by preys (Cranford et al., 2012).

5.1.   *Structural property*

The structure of spider silk is hierarchical, starting from nanostructure to macrostructure, and consists of amorphous network chains and β-sheet crystals constructed by poly-(Gly-Ala) and poly-Ala domains (Ackbarow et al., 2007; Keten et al., 2010). Some of previous works (Mita et al., 1994; Colgin and Lewis, 1998; Hayashi and Lewis, 1998) dedicated to reveal the genetic information on the amino acid sequence motifs present in spider fibroin. Basing on these work, Gosline et al. (1999) reported the molecular structure of spider silk, and analyzed its mechanical properties. Also, basing on scanning electron microscope and atomic force microscope images, Du et al. (2006) reported a new hierarchical model of spider silk (see Fig. 16). However, due to the existing experimental technologies, we cannot directly test the mechanical properties of each hierarchy of the silk. To this end, Buehler and his colleagues (Ackbarow et al., 2007; Buehler and Ackarow, 2008; Keten et al., 2010; Nova et al., 2010; Bosia et al., 2010; Giesa et al., 2011) made a huge amount of numerical studies to reveal the influence of hierarchical structures on mechanical properties of protein using molecular dynamics simulations; their first molecular-level structural analysis of protein assemblies (Keten and Buehler, 2010) was reported by developing a 3D model of silk's nanocomposite structure. In particular, the MaSp1 and MaSp2 proteins subjected to mechanical loading were studied, and the
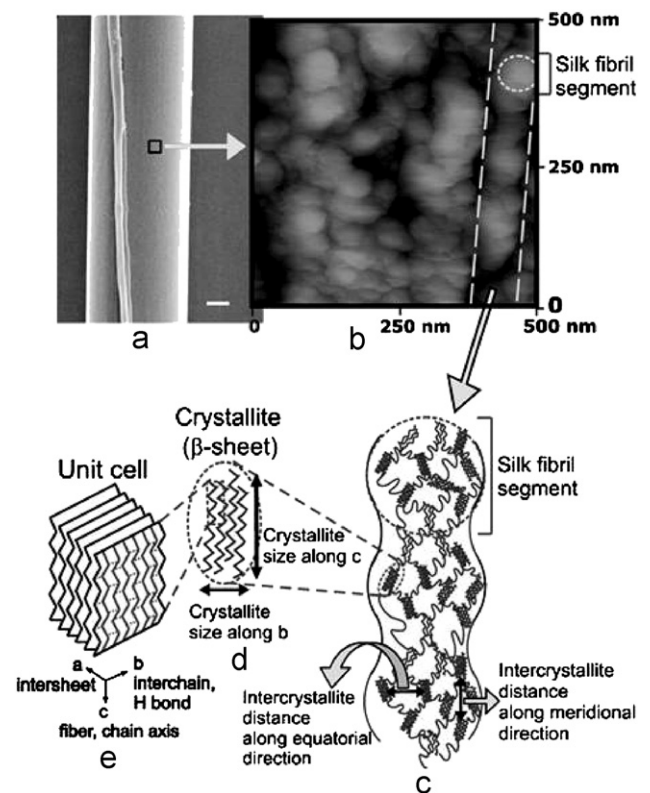
Fig. 16 – Hierarchical structure of a spider silk. (a) SEM image of spider dragline silk; (b) AFM image of silk fibril structure; (c) schematic of silk fibril structure; (d) schematic of crystallite; (e) unit cell of silk (Du et al., 2006).

results showed that the nanoscale behavior of the silk protein assemblies is controlled by the distinctly different secondary structure content and hydrogen bonding in the crystallite and amorphous regions. With these studies, they believed that the hierarchical architecture and seamless integration of
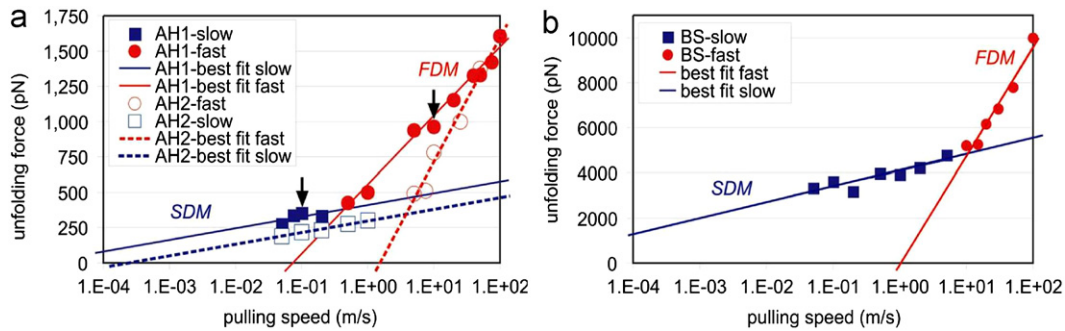
Fig. 17 – (a) Unfolding force of α-helical domains (IHBs) vs. pulling speed; (b) unfolding force of β-sheet domains (SHBs) vs. pulling speed (Ackbarow et al., 2007).

material and structure, from nano to macro, plays an important role in the structure–property relationship of spider silk and a direct comparison between experiment and simulation was reported (Keten and Buehler, 2008).

5.2. Toughening mechanisms

The excellent mechanical properties of spider silk are attributed to the co-action between different hierarchical levels. In terms of chemical composition and morphological structure, Porter et al. (2005) assumed that stiffness and strength, on the one hand, are due to the high cohesive energy density of hydrogen bonding, and toughness, on the other hand, is due to the high energy absorption during post-yield deformation; they employed mean field theory to study structure–property relations of spider silk. At nanoscale (hydrogen-bond level), Ackbarow et al. (2007) proposed two fracture mechanisms of biological protein materials by atomistic simulations (Fig. 17) on three protein structures (AH1, AH2 and BS), i.e., the unfolding mechanism at fast pulling rates invokes the rupture of individual hydrogen bonds (IHBs) (Fig. 17a) and unfolding at slow pulling rates proceeds by simultaneous rupture of several HBs (SHBs) (Fig. 17b), which is a typical structure of the lowest level. As for the influence of proline, the thermo-elastic measurements (Savage and Gosline, 2008) were employed to study it in the elastic mechanism of hydrated, spider silks and different structural organization in glycine-rich network chains and the mechanism of elasticity in proline-rich; proline-deficient fibroins resulted in different mechanical properties. Finally, the different strain-hardening behaviors of spider and silkworm silks were attributed to the unfolding of the intra-molecular β-sheets in silk fibrils (Fig. 18; Du et al., 2011), which is similar to the unfolded loops/domains of organic proteins between platelets in nacre. The mechanism is that protein backbones and nodes of the molecular network are stretched to support the load as the progressive unfolding and alignment of protein during fiber extension occurs. The process was described by Euler (2008) as entropy springs, which played an important role in soft matter and underlined the intriguing mechanical properties of spider silk.

As for the influence of crystal regions (Huemmerich et al., 2004), Du et al. (2006) reported that high strength of the spider dragline silk could be obtained by decreasing the size of the crystalline nodes in the polypeptide chain network while increasing the degree of orientation of the crystalline nodes.

Keten et al. (2010) revealed that the strength of spider silk arose from that of the β-sheet nano-crystals, and this is counter-intuitive due to the weak hydrogen bond, but they owed this result to nano-confinement and flaw tolerance (Qin and Buehler, 2011; Giesa et al., 2012), which improved the overall strength, toughness and stiffness. Also, Cetinkaya et al. (2011) used a bottom-up approach and combined molecular dynamics and finite element to analyze the effect of crystalline subunit size on the silk mechanics, and they reported that silk's Young's modulus and toughness increased with the crystal length but decreased with the crystal cross-section area; in particular, they considered both the crystalline and amorphous subunits, and concluded that the friction between entangled chains caused higher stiffness and energy absorbance, which homogenized the stress distribution.

Different from the separate studies on spider silk and web, Cranford et al. (2012) explored the relationship between the constitutive law of the silk and the robustness of the global web. In this work, combining atomistic simulations, theory and experiments, the authors found that the web robustness was improved by considering a realistic (i.e. hyper-elastic) more than elastic or elastic–plastic silk constitutive law; it causes a smaller localizing damage due to a local loading. Besides, the global behavior of the spider web was also illustrated by considering winds with different speeds. Finally, they concluded that the remarkable mechanical properties of individual spider silks were not the dominating reason providing the excellent performance of the spider web, but the nonlinear softening and subsequent stiffening of the silk play an important role in maximizing the web robustness.

Besides the mechanisms stated above, there are other environmental conditions influencing the mechanical properties of spider silk, such as spinning conditions, humidity and temperature. As for the spinning conditions, Pérez-Rigueiro et al. (2005) developed a forced silking procedure, which could measure the low force involved in the silking process, and found that fibers spun at high silking force were stiffer whereas fibers spun at low or very low silking forces were more compliant, of which tensile behavior corresponded to that of natural fibers spun by spiders; Liu et al. (2005) obtained the same result (Fig. 19a). Meanwhile, Yang et al. (2005) reported that the combination of high tensile strength and high extensibility provides spider silk a high toughness at low temperature, the conclusion can be seen in Fig. 19b: when the
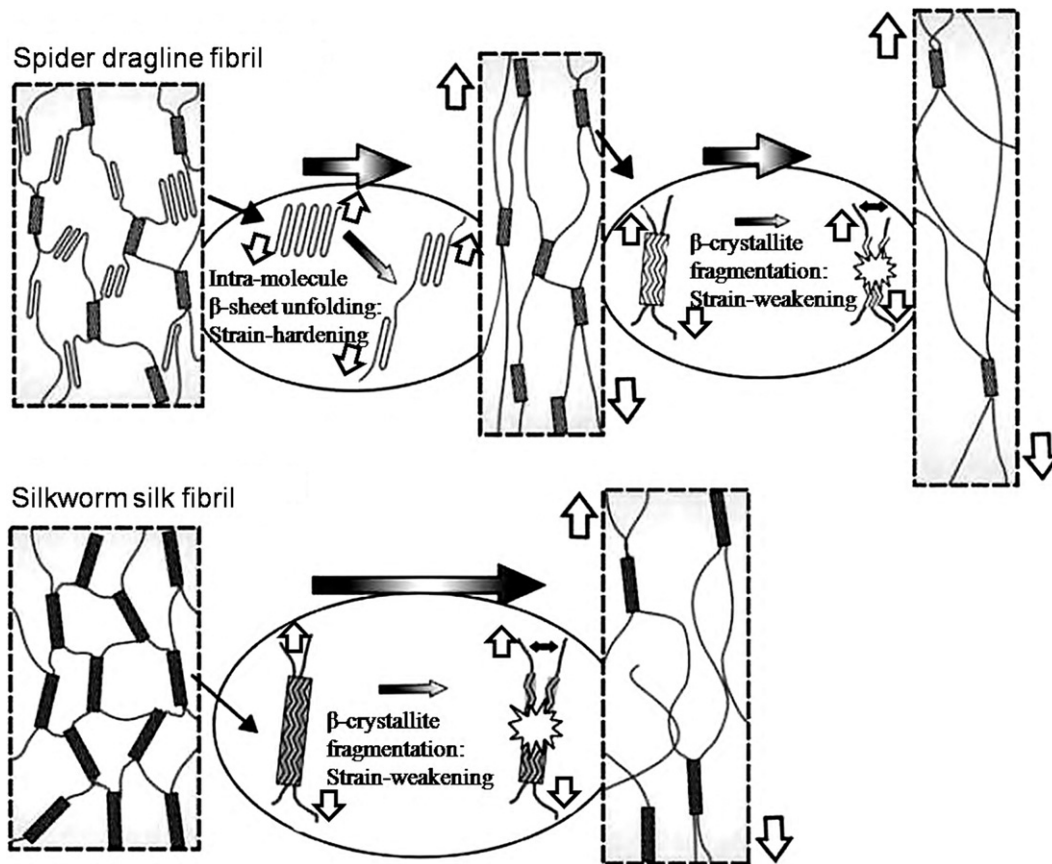
Fig. 18 – A schematic model demonstrating stretching difference between silkworm and spider dragline fibers (Du et al., 2011).

temperature increased from 15° to 150°, the strain-stress behavior changed a little, while the temperature decreased from 15° to −60°, the silk strength and extensibility increase dramatically. Agnarsson et al. (2009) performed two types of tests to examine the influence of water on the mechanical properties of spider silk, which is so-called "super-contraction" (Work, 1977), and found that the cyclic humidity caused the cyclic stress response (Fig. 19c), which induced the contraction and relaxation in drying and wetting environments, respectively. From the viewpoint of the evolution, Boutry and Blackledge (2010) explained the mechanism of super-contraction in spider silk, which was induced by a rearrangement of GPGXX motifs, and found the structure–function relationship to tailor the silk properties. Finally, Venner and Casas (2005) explored the relationship between the size of prey and the spider web, and reported that spiders could not survive or produce eggs without catching large but rare preys and increasing web size increases the daily number of prey caught and thus long-term survival and fecundity.

Theoretically, Zhou and Zhang (2005) developed a hierarchical chain model (Fig. 20a) with different motifs at different levels to investigate spider silk strength and elasticity (Fig. 20b; Becker et al., 2003). In this model, two elements were considered: the closed parts denote crystallites and the broken or solid lines denote bonds or amorphous biopolymers. The proposed model is supported from the amino-acid sequence of the major flagelliform protein of spider capture silk. Ackbarow et al. (2007) employed

the hierarchical Bell model to express a rigorous structure–property relationship from the point of view of statistical mechanics. Bosia et al. (2010) adopted a newly developed fiber bundle model approach with a hierarchical multi-scale self-similar procedure to consider the hierarchical topology of natural materials; to some extent, they explained the energy dissipation mechanisms. Recently, Pugno and his colleagues (Pugno et al., 2012), basing on the Daniels' model on fiber, developed a new theory to predict the mechanical strength of a hierarchical fiber bundle model, which could be used to model spider silk; in particular, they considered the complex architectures of biological materials, including size effect, twisting angle and friction. Interestingly, the combination of structural hierarchy and different materials mixing can result in a higher mean strength, which cannot be achieved by only hierarchy in a homogenous phase (Bosia et al., 2012).

6.   Exoskeletons of lobsters/crabs

Lobster or crab cuticle (Fig. 21) is another widely-studied natural material with high mineralization, which is divided into three layers, i.e., epicuticle, exocuticle and endocuticle (Fig. 21VII). These layers, from exterior to interior, have decreasing densities (Raabe et al., 2005a,2005b). Fabritius et al. (2009) systematically analyzed the studies of lobster and elaborated the structural and mechanical properties of
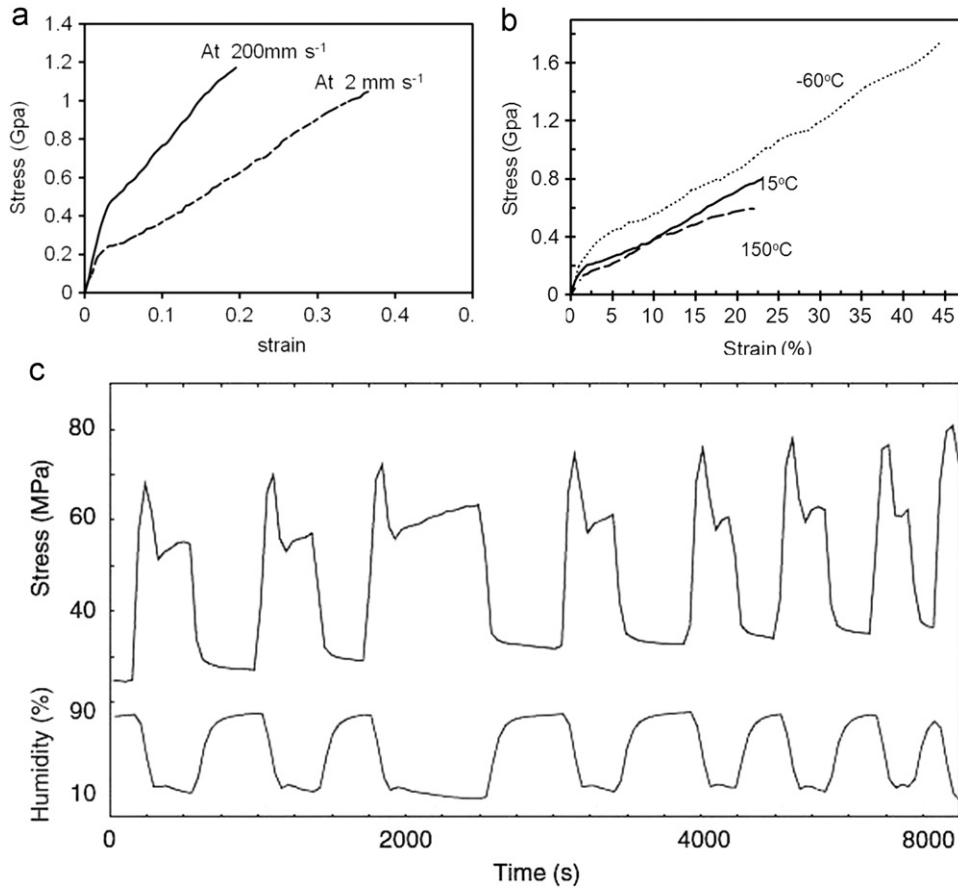
Fig. 19 – (a) Silk spun at 2 mm/s vs. that at 200 mm/s (Liu et al., 2005); (b) the influence of temperature on web-building speed (Yang et al., 2005); (c) dragline silk repeatedly contracts and relax with humidity (Agnarsson et al., 2009).
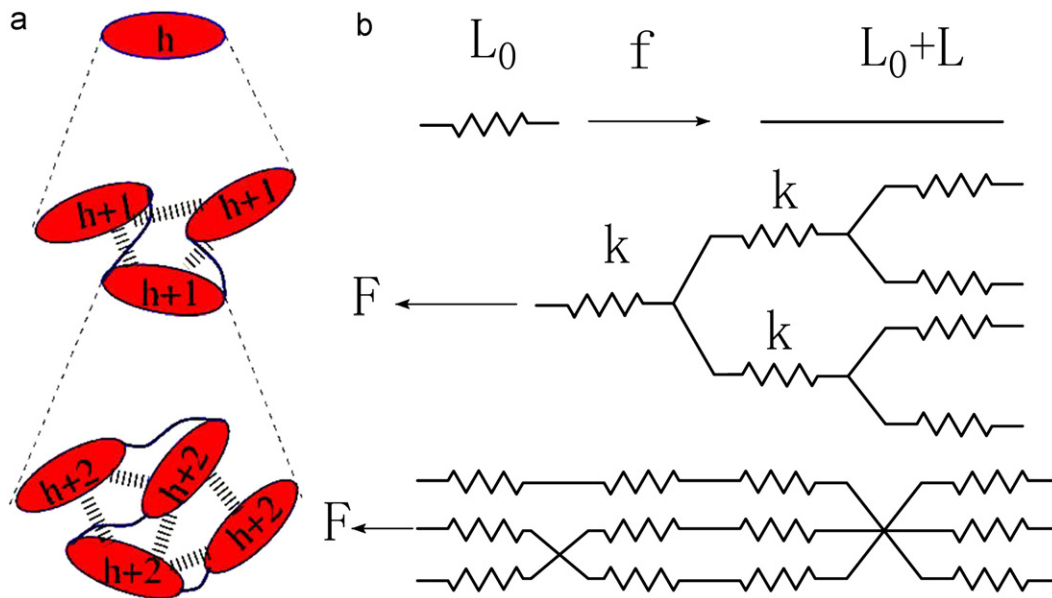
Fig. 20 – (a) Hierarchical chain model, the broken lines denote sacrificial bonds and the solid ones denote surviving bonds (Zhou and Zhang, 2005); (b) schematic of a network of identical springs in spider silk (Becker et al., 2003).

the biological composites. Firstly, the twisted plywood or Bouligand structure (Fig. 21VI), which is frequently encountered in Nature, especially in the skeletal and protective mineral tissue (e.g. compact bone), is the prominent building

principle to develop the mechanical behaviors of the biocomposite (Fabritius et al., 2009). Secondly, the honeycomb structure (Fig. 21V), which was formed by the interconnected fibers bend around the pore canals and discovered by Raabe
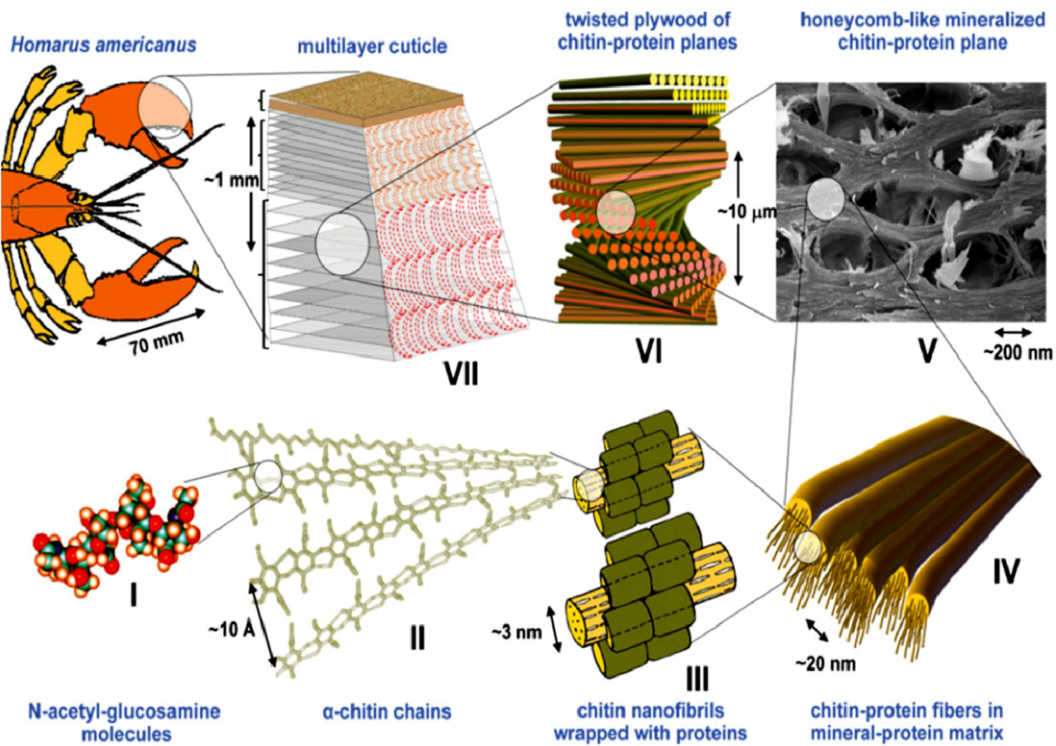
Fig. 21 – Hierarchical structure of the lobster cuticle (Nikolov et al., 2010).
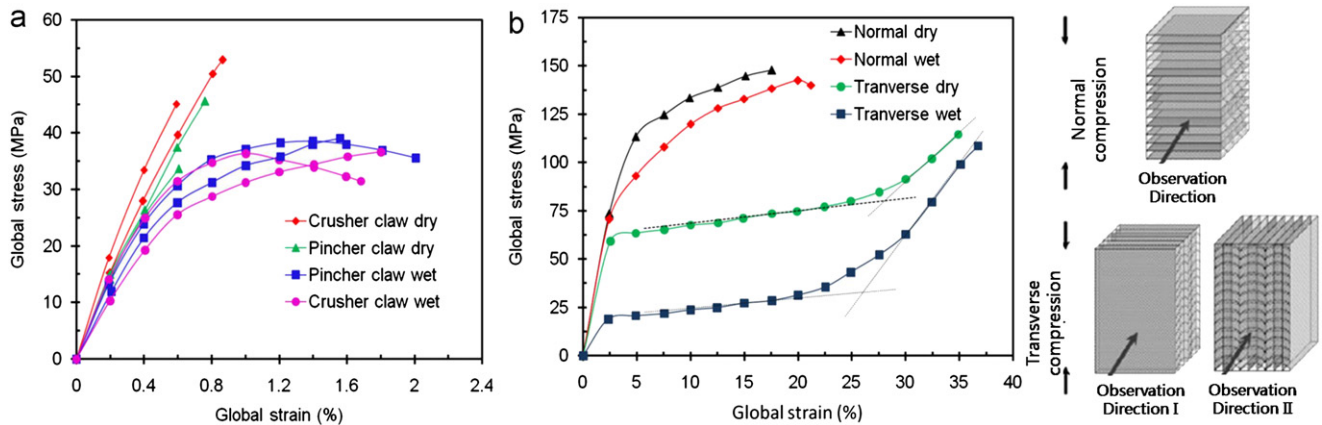
Fig. 22 – (a) Global stress–strain relationship of the endocuticle from the pincher and crusher claws both in dry and wet state under tensile loading (Sachs et al., 2006a); (b) global stress–strain relationship of the endocuticle and schematic figure of the compression tests (Fabritius et al., 2009).

et al. (2005a,2005b), is another important and effective building principle. Besides, Raabe et al. (2006,2007) studied preferred crystallographic texture of the α-chitin–protein network in the exoskeleton of the lobster and elucidated crystallographic building principles in crystalline organic tissue; in the end, they made a conclusion that complex hierarchical structure could be simply described by crystallographic textures.

As for the mechanical properties, Raabe et al. (2005a,2005b) studied the mechanical and structural gradients of the exoskeleton by experiments on stiffness and hardness; they found that, from outer layer to inner layer, the stiffness decreased from 9 GPa to 4 GPa or so and hardness from 130 MPa–270 MPa

to 50 MPa; they also pointed out that there was an important influence of the interfaces between layers on the overall mechanical behavior. Employing nanoindentation, Sachs et al. (2006a,2006b) and Romano et al. (2007) revealed gradient and anisotropy in the hardness of such dehydrated materials; in order to fully understand the mechanical properties of the natural material, Sachs et al. (2006a,2006b) continued to perform a tensile experiment on both dry and wet samples to examine elastic–plastic deformation behavior of the lobster cuticle, combining with a detailed global and local strain analysis (Fig. 22a); they found that the heterogeneity by local strain analysis and the existence of water both enhances the
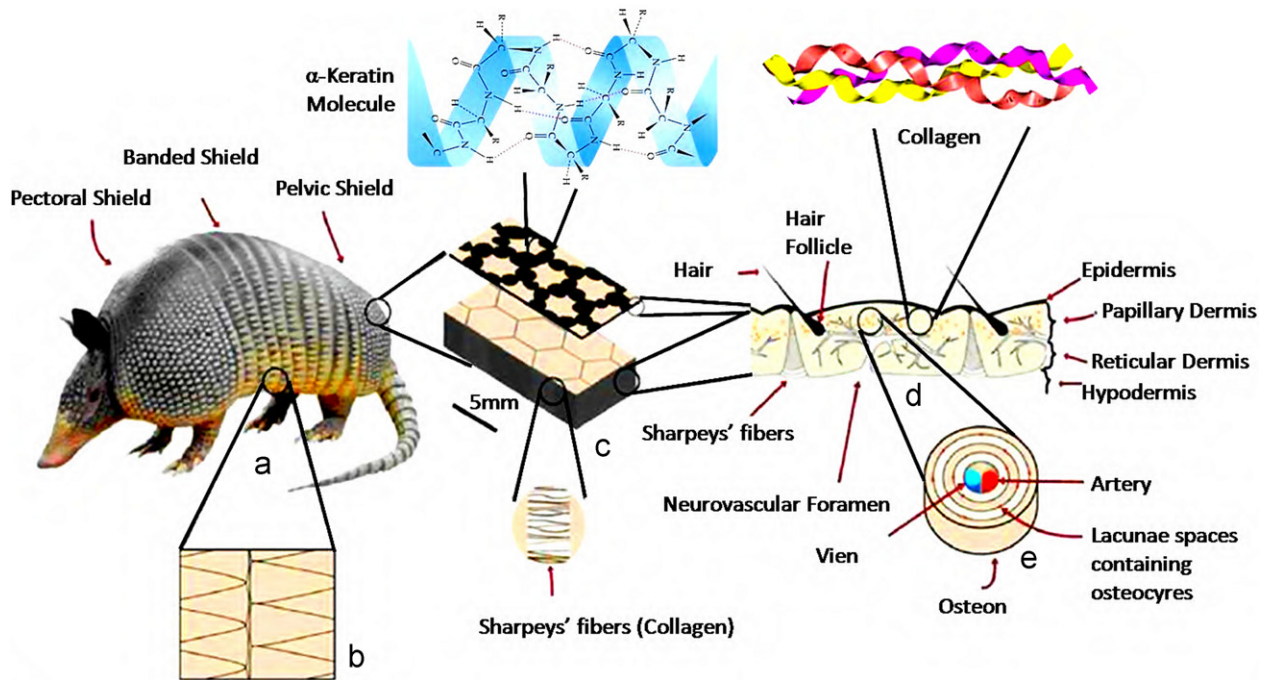
Fig. 23 – Hierarchical structure of the nine-banded armadillo's dermal shells. (a) Armodillo; (b) triangle scales of band shell; (c) hexagonal scales of rear shell; (d) cross-sectional view of rear shell (Chen et al., 2011).

plastic deformation ability. In addition, Sachs et al. (2008) illustrated the influence of microstructures on deformation anisotropy of the exoskeleton under different loading directions (Fig. 22b), i.e. in the normal direction (out-of-plane) to the cuticle and in the transverse direction (in-plane), which share the similar mechanical behaviors with conventional honeycombs (Papka and Kyriakides, 1994,1998a,1998b).

In particular, incorporating quantum mechanics and density functional theory, Nikolov et al. (2010) recently proposed a method to investigate structure–property relations of the lobster at all length scales and developed a hierarchical model: it included ab initio calculations at the nanometer scale and mean-field homogenization for higher hierarchy levels. By a bottom-up approach, Tang et al. (2009) and Chen and Pugno (2011a,2011b) derived the mechanical properties of a given hierarchical level starting from those of the lowest level, and by an iterative procedure, the properties at all length scales are obtained.

7.   Armadillo shell

Armadillo (Fig. 23), as a natural carrier of the leprosy bacillus, has been studied extensively and deeply for the immunology, chemotherapy, and epidemiology of the disease (Truman et al., 1991; Truman, 2008). Recently, as the emerging study of biological materials, its mechanical properties started to attract researchers' attention. Rhee et al. (2011) analyzed chemical elements using X-ray spectroscopy technique; basing on drying and ashing experiments, Chen et al. (2011) found that they contain 13.6 ± 0.4 (wt%) water, 64.8 ± 1.3 (wt%) mineral, and the remaining part is mainly composed by collagen and keratin. Here, we mainly focus on

the structural and mechanical properties of the armadillo's shell.

The structure of armor shell (or osteoderm) is divided into three types, i.e., forward shell (pectoral shield), band shell (banded shield), and rear shell (pelvic shield), Fig. 23a, which are formed by a number of overlapped scales with different shapes (triangle in the band and hexagonal in forward and rear shells). Addressing the microstructures of the three mentioned parts, Rhee et al. (2011) employed Scanning Electronic Microscope (SEM) to fully characterize them. The forward and rear shells (Fig. 24) share a common structural property, and both are sandwich composite structures; they contain a hard and dense exterior layer and a porous interior layer, which is similar to the structure of bone (Vickaryous and Hall, 2006) and turtle shell (Rhee et al., 2009). However, as for the band shell, it is more complicated and sophisticated (Fig. 25); each band is overlapped at the rear part of the anterior one and is thicker than that of the rear part (Fig. 25(i–l)); the structure of the thick forward part of each band is similar to those of the forward and rear shells but with larger pores (Fig. 25(e–h)), while the structure of the thin rear part of each band shows a regular single-layer wood-cell-like structure (Fig. 25(e–h)). Besides, the collagen (Sharpey's fibers) connects scales together, and enhances the armor flexibility by collagenous retraction to make the body bend (Fig. 26). This is different from that of nacre, in which the organic layer is mainly between calcium carbonate platelets, and the nacre has a weaker flexibility but with stronger in-plane strength and toughness, which depends on their functions of the tissues.

Regarding the mechanical properties of the shell, Rhee et al. (2011) employed Vickers hardness tester to test related tissue hardness, and Instron electromechanical test
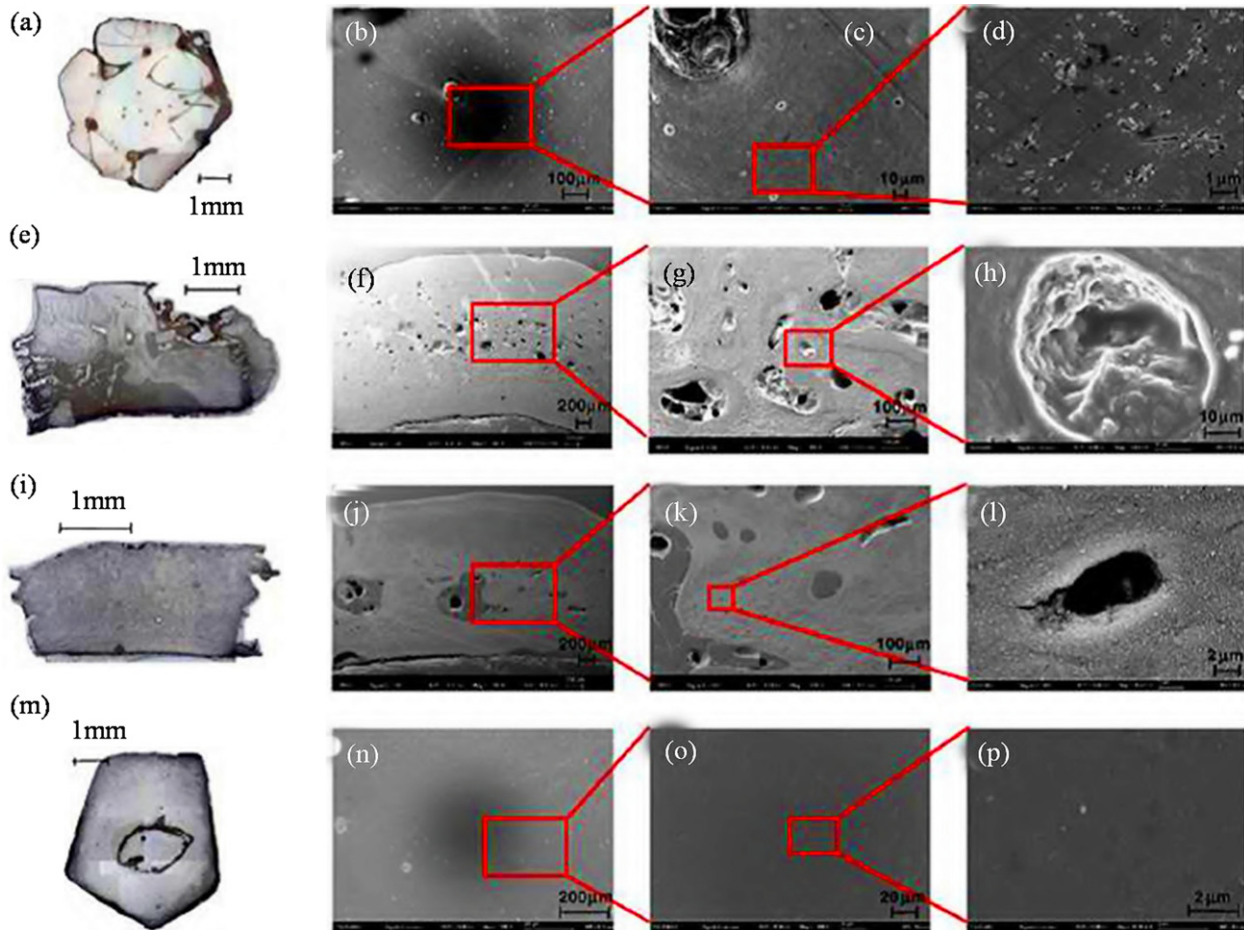
Fig. 24 – SEM images of the hierarchical structure of the forward shell: (a–d) top view; (e–h) front view; (i–l) side view; (m–p) bottom view (Rhee et al., 2011).

apparatus to test their strength. They found that the bottom and top surface were harder (~53 Hv) than the front and side surfaces (~45 Hv), which indicated denser surfaces; they also found that the strength of the forward shell (~1.5 GPa) was three times than that of the band shell (0.5 GPa), and the former mechanical behavior was akin to that of the foam materials (Gibson and Ashby, 1997); this is probably due to the inelastic deformation mechanism of micro-buckling while the intrinsic material behavior was approximately linear elastic. Chen et al. (2011) performed experiments on both dry and wet shell samples without considering which part the samples were from; they found that Young's moduli of the dry samples (~425 MPa) were almost three times than those of the wet samples (~150 MPa), tensile strength of the dry samples (~23 MPa) two times than those of the wet samples (~13 MPa), and toughness of the dry samples (~1.1 MJ/m^3) two times than those of the wet samples (~0.53 MJ/m^3).

8. Turtle shell

Turtle is one of the eldest vertebrates and is believed to have existed for 200 million years. Its shell, composed of a dorsal shell (carapace, usually a strong and rigid structure; Fig. 27) and a ventral shell (plastron), represents an evolutionary novelty (Gilbert et al., 2001; Krauss et al., 2009); it plays a significant role in physical protection and reserving water, fat, or wastes. Therefore, many works investigated the evolutionary and morphogenesis of its box-shell structure, from carapacial ridge-specific gene to embryonic development of the shell and biologists try to uncover how turtle forms its shell (Kuraku et al., 2005; Rieppel, 2009). Recently, Rhee et al. (2009), using an energy dispersive X-ray (EDX) technique, analyzed the chemical elements existing in the outermost keratin layer, the layer right underneath the outermost keratin layer and the inside surface of the carapace shell. However, as for the armadillo shell, the microstructure–mechanical relationship has not been studied extensively, and so we here review the pioneering works, only recently developed, on the shell microstructure and its mechanical properties.

It is recognized that the structure of the carapace shell is a sandwich structure (Balani et al., 2011), like that in the armadillo shell (discussed above). The sandwich structure consists of two thin but dense layers, which are known as endocortical and exocortical bone layers, and the porous trabecular bone, which can be often found in bones of other species (Krauss et al., 2009). The carapace shell is formed by
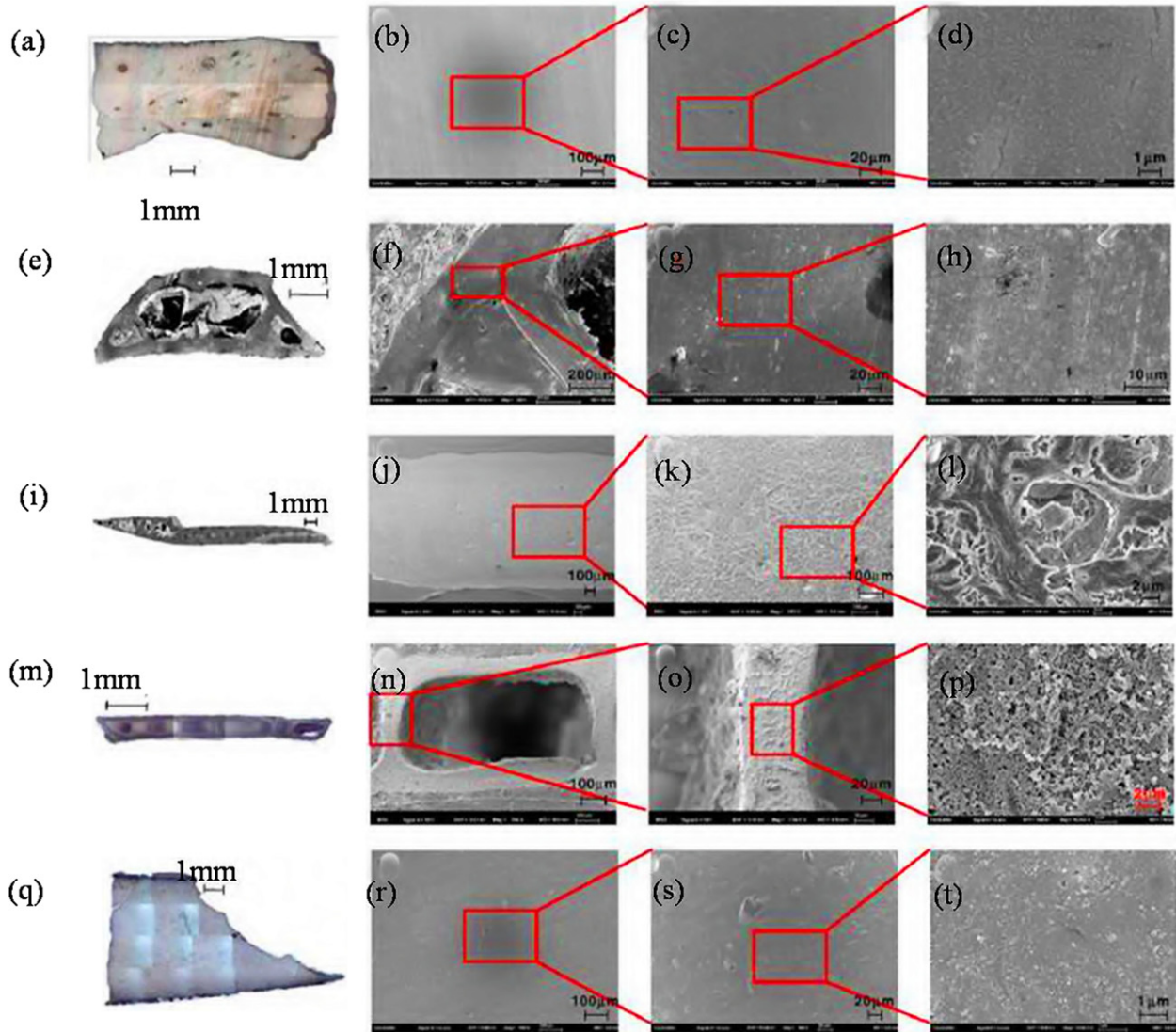
Fig. 25 – SEM images of the hierarchical structure of the band shell: (a–d) top view; (e–h) front view; (i–l) side view; (m–p) back view; (q–f) bottom view (Rhee et al., 2011).
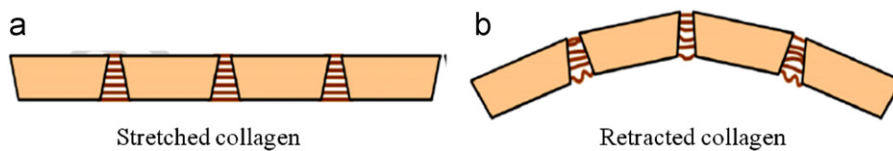
Fig. 26 – Schematic of connection between tiles and collagen fiber (Chen et al., 2011).

series of individual plates, which are connected by zigzag joints (interlocking mechanism) and covered by a layer of keratinized scutes, which is the β-keratins (also found in armadillo, and crocodilian; Rhee et al., 2009; Valle et al., 2009), which acts as a 'glue' to connect individual scutes together. Interestingly, Krauss et al. (2009) investigated the joint area (Fig. 28a) in detail (50–80 μm wide, 150–180 μm long, and rotated by 35–45° with respect to the normal axis of the shell surface), and reported that the interlocking joint enabled turtles to move flexibly and bear high-magnitude impact loading when attacked by predators; they also presented a

fundamental concept of structure–mechanics relationship to explain how the shell functions when imposed by loads with different magnitudes. Balani et al. (2011) explicitly illustrated the multi-functionality of turtle's carapace (Fig. 28b): (i) the waxy layer on the surface is for slipping away from predators and reducing drag force while swimming, (ii) the third dense layer provides further shielding, (iii) multilayer and porous structures absorb shock caused by fall, and (iv) porous structure stores nutrient and fluids.

Mechanical investigation was carried out by Krauss et al. (2009) to reveal the mechanical function of the suture (joint
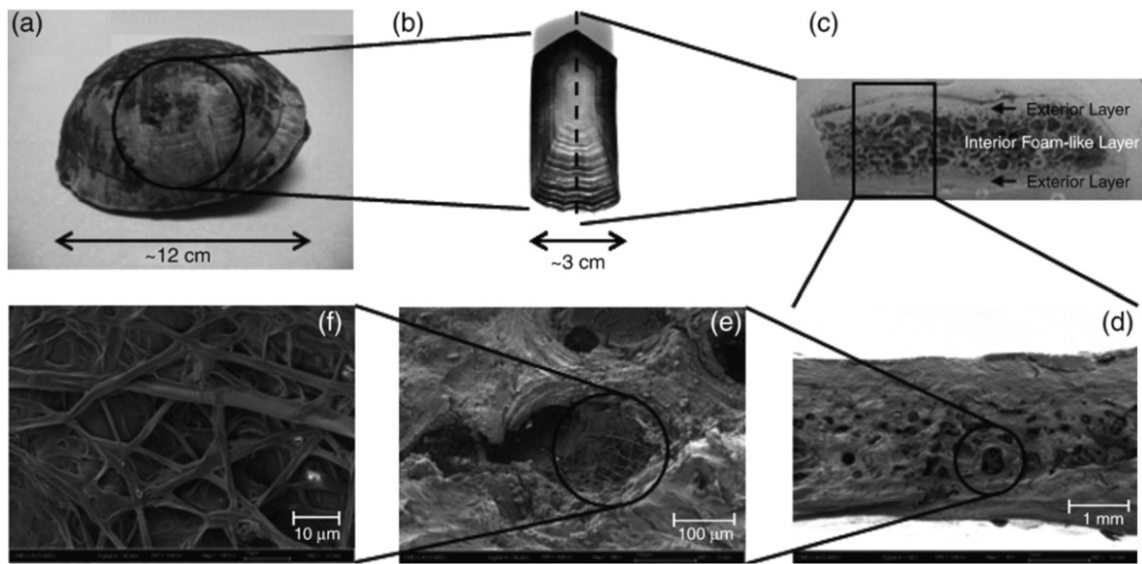
Fig. 27 – Hierarchical structure of carapace shell: (a) the turtle carapace shell; (b) a costal scale; (c) form-like cross-sectional view; (d) a SEM image of cells; (e) a magnified SEM image of cells; (f) fibrous structure inside a cell (Rhee et al., 2009).
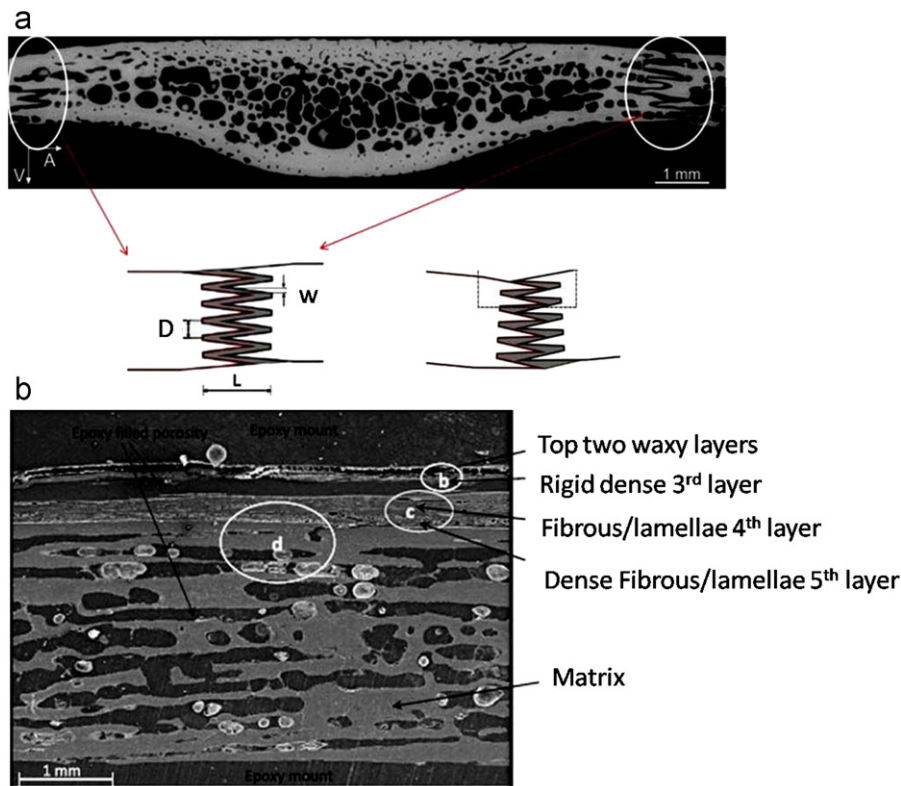
Fig. 28 – (a) Sandwich structure of turtle carapace, schematic of the interlocking joint and micromovement of the joint (Krauss et al., 2009); (b) multilayers structure of turtle's carapace (Balani et al., 2011).

area) in the deformation process by a three point bending experiment, and the results showed that the stiffness of the samples with suture was low in the initial phase (slight movement due to walk) and gradually transited to a high stiffness as loads increased (external attack), while the stiffness of the samples without suture started with a high value (Fig. 29a). The behavior provided a good explanation

about the mechanical properties during the locomotion and protection. Rhee et al. (2009) performed hardness, compression and flexure tests, respectively; they reported that the hardness of the exterior and interior layer of the sandwich structure were comparable ($\approx$1 GPa) similar as their elastic modulus ($\approx$20 GPa); Balani et al. (2011) reported the same results on Young's moduli and strengths of different layers.
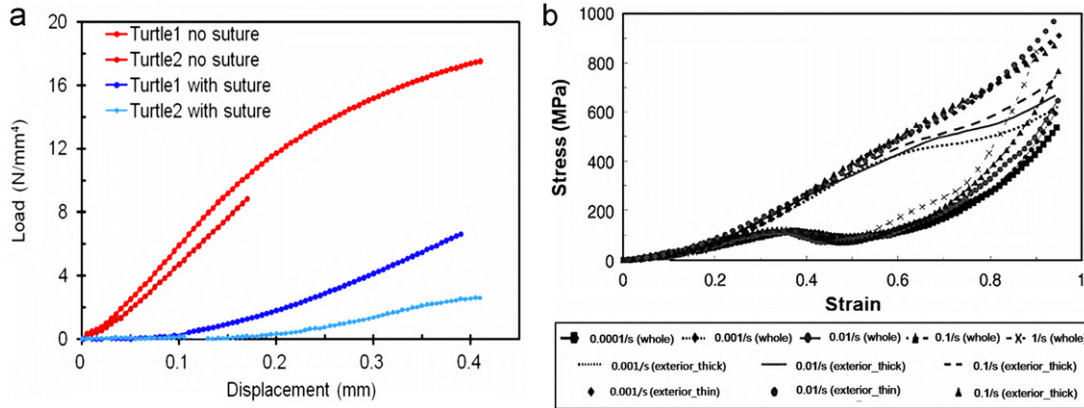
Fig. 29 – (a) Mechanical function of the suture (Krauss et al., 2009); (b) the constitutive curves of the sandwich structure, single interior layer, and single exterior layer (Rhee et al., 2009).
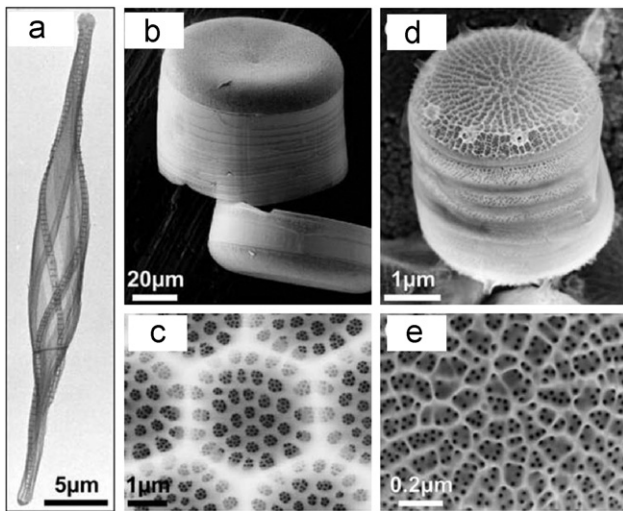
Fig. 30 – Hierarchical structures of diatom cell walls. Electron microscopy images of isolated cell walls from different diatom species: (a) *Cylindrotheca fusiformis*; (b,c) *Coscinodiscus asteromphalus* and hierarchical sieve plate; (d,e) *Thalassiosira pseudonana* and hierarchical sieve plate (Sumper and Kröger, 2004).

The deformation mechanism was attributed to the middle porous layer which had a similar behavior as that of honey-combs, i.e. linear-elastic phase (due to trabecular beam bending), platform phase (trabecular beam buckling), and densification phase (trabecular beam crushing; Papka and Kyriakides, 1994; Gibson and Ashby, 1997), but the single exterior and interior layers have no platform (Fig. 29b).

9.   Diatoms

Diatoms are unicellular eukaryotic algae that exhibit silicified cell walls with hierarchical structures from nano- to meso- to macro-scale and a diversity of species (Sumper and Kröger, 2004; Fig. 30). The cell walls called frustule possess a high toughness and strength due to intricate symmetric and duplicable architectures to resist potential threats from their surrounding environment, although the basic constituent

materials are silica which are always fragile (Hamm et al., 2003). To this end, many contributions (Hildebrand et al., 2006; Losic et al., 2007; Hildebrand et al., 2008) started from the morphology to characterize the forming process of the optimized structure by different experimental devices, such as atomic force microscopy (AFM), scanning electron microscope (SEM), transmission electron microscopy (TEM), and recent publications (Garcia et al., 2011a,2011b) also reported the mechanism of the high toughness in the frustule.

The forming process of the valve structures generally includes three steps (taking *T. pseudonana* as an example; Fig. 31): (1) at the beginning, the base layer of the valve is developed by depositing fractal-like branching ribs of silica (Fig. 31b); (2) then, the silicification (Fig. 31c) starts from the central part to the peripheral part; in this dynamic growth process, the organic components—silaffins and polyamines—exert a considerable influence on the silica biogenesis (Sumper and Kröger, 2004) and the actin filament plays a vital role in inducing the biogenetic path (Tesson and Hildebrand, 2010). In this regard, we have to briefly discuss another marine creature, i.e. seasponge. The formation of its hierarchical skeleton structure is also guided by the axial filament on which the silica is deposited (Aizenberg et al., 2005); the structural formation steps are explained in detail by Weaver et al. (2007). These two structures share a common characteristic of biomineralization and it is just its action that endows diatom structure with high toughness and ductility, by combining some weak constituent materials. (3) Subsequently, the silicification continues and the ribs of the valve become more rigid, and thus form mature individual diatom. Fig. 31d, e shows that the proximal end of the mature valve is smooth while the distal end is rough, strengthened by branching ribs; Fig. 31f, g shows the AFM images for the proximal and distal ends of the valve, respectively; interestingly, the 50 nm spherical silica particles topping the ridges can be easily recognized, which are the result of the silica biogenesis.

As for the formation of the girdle band, it is not clear due to the difficulty of the thin structure; therefore, rare images are captured to illustrate its structural formation, even if several studies indicate that girdle bands exhibit similar complexity in
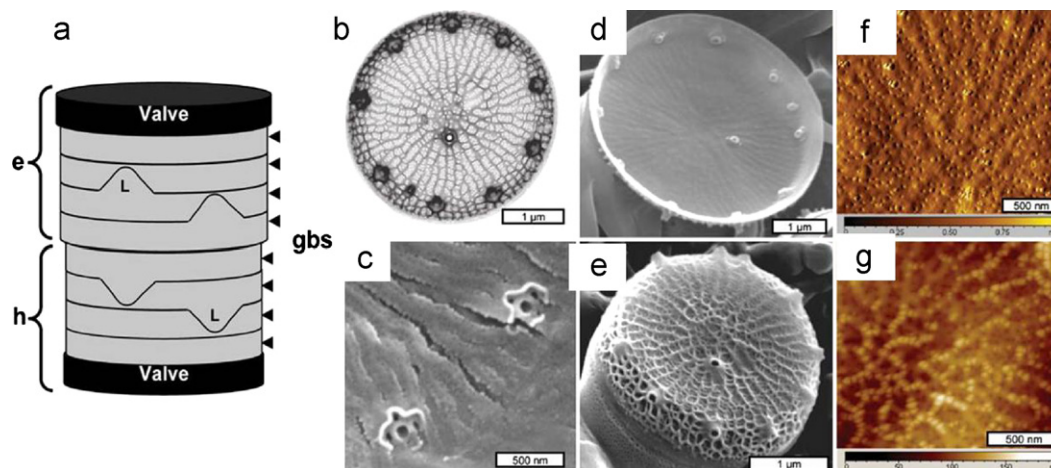
Fig. 31 – (a) Schematic of the cell-wall structure, the upper part e is the epitheca and the lower h the hypotheca, the extreme upper and lower portions are valves, which are the silica structures, gbs are silicified girdle bands encircling the cell, L is ligula with bell shape. (b) TEM of *T. pseudonana* valve showing the branched rib structure. (c) SEM of developing valve ribs with flattened nature. (d) SEM of smooth inner (proximal) valve surface. (e) SEM of rigid outer (distal) valve surface. (f) AFM of the proximal valve surface. (g) AFM of the distal valve surface (Hildebrand et al., 2008).

their structure and formation processes as some valve structures (Hildebrand et al., 2009; Tesson and Hildebrand, 2010).

Addressing the brittle constituent materials-silica forming such hierarchical structures, the integration of the different structures, spanning different length-scales, determines its excellent mechanical properties. In particular, the silica nanostructure is considered to yield a superior toughening mechanism (Garcia et al., 2011a,2011b). Thus, Buehler's group studied the geometrical nanostructures of different diatom species, such as the helical silica (Mohedas et al., 2011; Fig. 32a, b) nanostructure in *Rutilaria grevilleana* and the wavy silica nanostructures in the girdle band of *E. arenaria* (Garcia et al., 2011b; Fig. 32c, d) by atomistic simulation tools. The toughening mechanisms of the two structures are contributed to the pull-straight or uncoiling effect, which produce more than 100% Cauchy strain. It is worth mentioning that in Fig. 32a, the upper coil belongs to one valve and the lower coil belongs to the other valve, which is different from the model in Fig. 32b and is not a helical (or spring-like; Mohedas et al., 2011; Gebeshuber et al., 2009) structure, but indeed the extension and compression and of the coils could absorb energy produced by impact, forces or even rotation (personal communication with R.W. Crawford). Not confined by the two, another nanohoneycomb structure was also studied finding two competing mechanical behaviors: shear deformation or brittle crack propagation (Garcia et al., 2011a). From Fig. 33, we can see that when the width of cell walls in the nanostructure increases, the toughening mechanism varies from the pure shear deformation ($w < 21$ Å) to shear and crack coupling (21 Å $< w < 62$ Å) up to pure crack propagation ($w > 62$ Å); the optimized value is obtained when the width approximately is 40 Å and the shear deformation dominates (Fig. 33a). The Cauchy strain can reach 65% thanks to the structural change, from rectangular to hexagonal grid (Garcia et al., 2011a; Fig. 33b); accordingly, the crack tip opening displacement drastically increases from 0 up to 50 Å, which equals the width of the cell wall; thus, the structure apparently
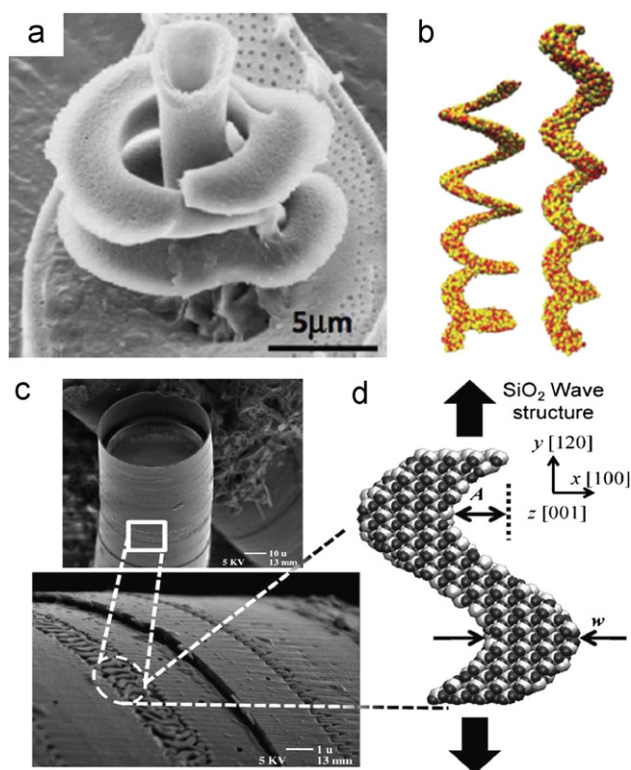
Fig. 32 – (a) Typical structure in *Rutilaria grevilleana*, © R.M. Crawford, AWI Bremerhaven, Germany; (b) model of the helical silica nanostructure (Mohedas et al., 2011); (c) *E. arenaria* showing a wavy structure in the girdle band; (d) model of the wavy structure (Garcia et al., 2011b).

undergoes plastic shear deformation and produces necking phenomenon (Fig. 33c). At the same time, flaw-tolerance and surface effects (Gong et al., 2012; Chen and Pugno, 2013) improve structural ductility, strength and toughness (Sen et al., 2011).
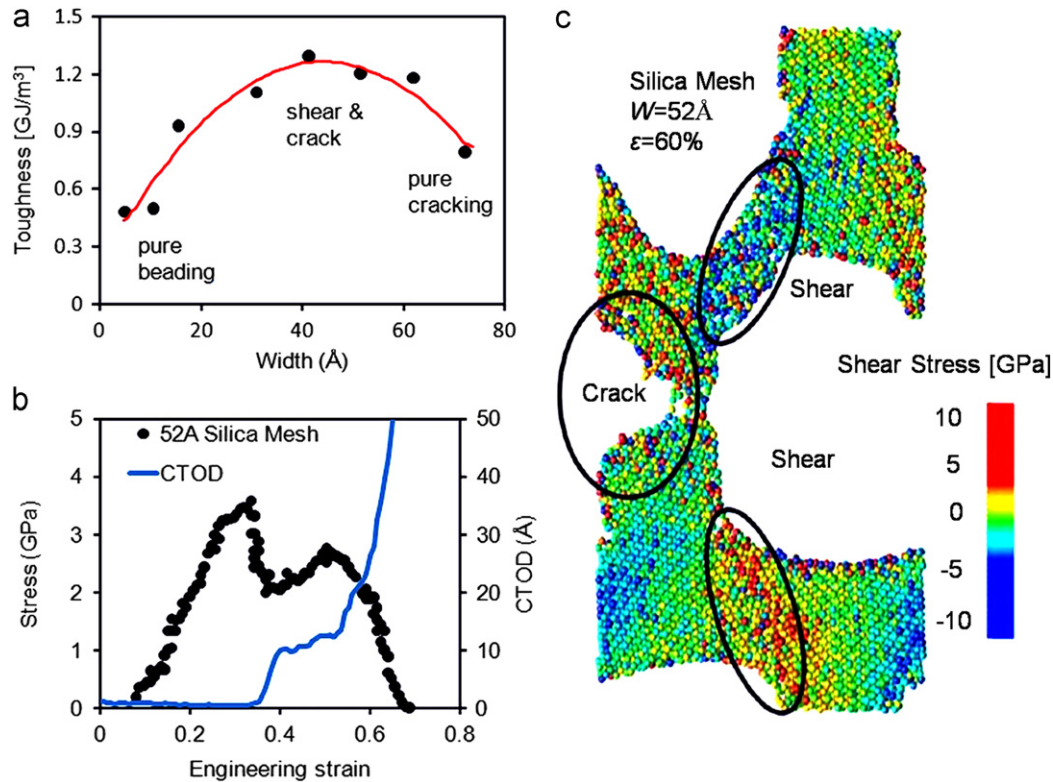
Fig. 33 – (a) Toughness map with corresponding failure mechanisms for the silica mesh with different cell wall widths; (b) toughening mechanisms are caused by competing mechanisms of shear deformation and crack formation. The crack tip opening displacement (CTOD) measurement reveals crack arrest and is plotted against the corresponding stress–strain data; (c) locations of shear deformation and crack propagations (Garcia et al., 2011a).

10.   Plant stem

Plant stem provides the mechanical support in order to adapt to surrounding mechanical environment and acts as channels to transport water and other nutrients. We can understand this easily by imagining that the plant stem carries torque/bending moment and vibrates when wind comes. Most of plant stems are circular and porous structure (Bejan, 2000), e.g. tree stem and grass stem (Fig. 34); this is because the circular shape possesses the largest area compared with other polygons under the condition of the same perimeter and the porous architecture has the low-weight and stronger energy-absorbing properties.

The structure of plant stems was treated as a cylindrical shell with foam by Karam and Gibson (1994)—the outer shell was full of dense materials and porous structure was the core (Fig. 34a); meanwhile, the elastic buckling behavior of the thin-walled structure was analyzed by theoretical investigation (Karam and Gibson, 1995a) and verified by experiments (Karam and Gibson, 1995b); from these results, there is great potential for biomimicking engineering structures, because the honeycomb/foam shell structures could substitute stiffened shells by improving the structural efficiency, and the new compliant shell can reduce the sensitivity to intrinsic imperfection providing high theoretical buckling stress. Basing on the thin-walled tubes/shell, Niklas (1997a,1998) examined

material properties (Young's modulus, critical shear stress, etc.) of stem tissues by examining the mechanical behavior of hollow internodes with transverse nodal septa subjected to bending and twisting, and an important conclusion drawn is that the mechanical behavior of the hollow, septate stems is more correlated with internodal shape than with the absolute length, wall thickness, and external radius of internodes; also, he studied the vibrating responses of the tube stem with node (e.g. bamboo) and found that the nodes acted mechanically like a series of spring, which could be used to store strain energy except stiffening the hollow cylindrical structure (Niklas, 1997b). In order to determine if sclerenchyma cells are the main components that resist stem bending and the mechanical properties of stems, Evans et al. (2007) studied 42 species of grass plants and discovered that 59% of all sclerenchyma cells in stems occur in the outer one-fifth radius of stems (Fig. 34b), which is the main support for stem integrity.

As for the structural efficiency, Wegst and Ashby (2007) optimized the mechanical properties of orthotropic tube, stalk and stem, which included the shape and anisotropy, by considering stiffness, strength and failure by ovalisation, instability and local kinking. Incorporating heterogeneity and high anisotropy, Schulgasser and Witztum (1997) investigated the strength of vascular plant stems and they reported that the plant stem sacrifices the strength and vertical stability in order to reduce the external bending moment (Fig. 35), which is the so-
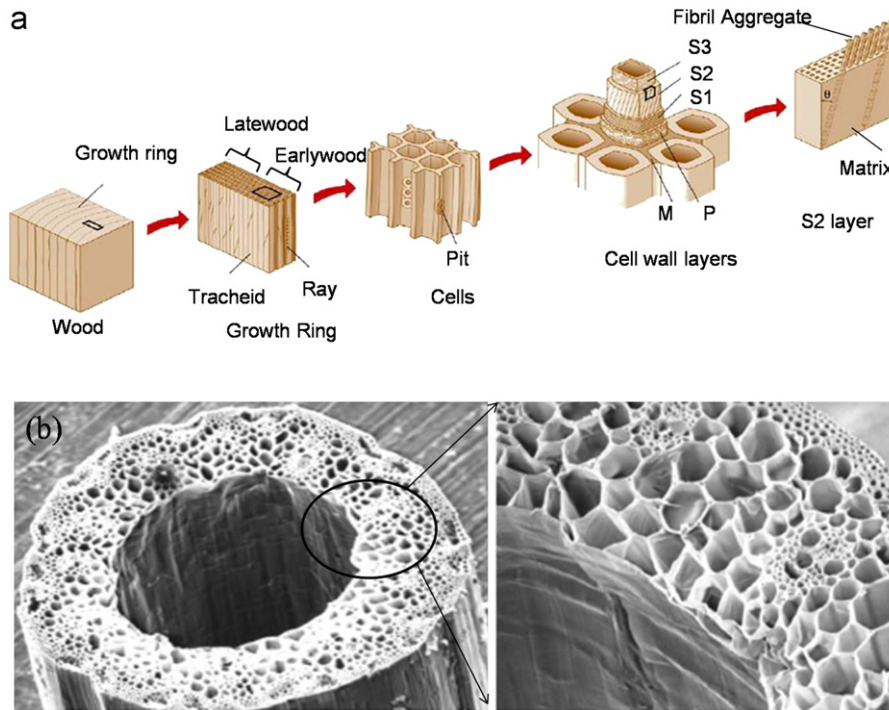
Fig. 34 – (a) Schematic of hierarchical structure of wood (Rafsanjani et al., 2012); (b) structure of grass stem (Gibson, 2005).
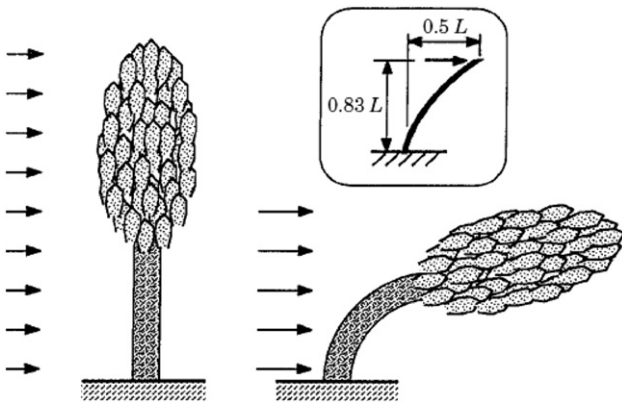
Fig. 35 – Simple model of passive automatic adjustment (Schulgasser and Witztum, 1997).

called "passive automatic adjustment" mechanism; also as the height increases, the plant tends to develop a high anisotropic tissue arrangements in order to gain high bending stiffness to maintain its stability. For the mechanics of natural cellular materials, which is one type of the four kinds of natural materials, Gibson (2005) reviewed their mechanics and discussed their roles in natural sandwich structure (e.g. skull, trabecular bone) basing on their developed theory (Gibson and Ashby, 1997).

Here, we discuss out-of-plane mechanical efficiency for circular and hexagonal honeycombs, see Fig. 36a, and according to their geometries the critical condition is computed in Fig. 36b. We can see that under the line the circular honeycomb is more efficient than the hexagonal one whereas above the line the opposite is true.

The hexagonal honeycomb (Fig. 37) is often modeled considering a unit cell and following the well-known theory by

Gibson and Ashby (1997); recently, Chen and Pugno (2012a) completed the theory addressing the in-plane buckling property of the structure, which shows the buckling possibility of the inclined cell wall in a hexagonal honeycomb. Regarding hierarchical structure of the wood (Fig. 34a), Hofstetter and Gamstedt (2008) reviewed the developments in the field of hierarchical modeling of the hygro-elastic behavior of wood. They focus on composite micromechanical models for the wood cell wall and on multi-scale models for wood resting upon hierarchical finite element models; meanwhile, they pointed out that to understand fundamental aspects of wood required taking into account the heterogeneity, anisotropy and hierarchies. Qing and Mishnaevsky (2009) built a 3D hierarchical model (Fig. 37a) with heterogeneous multiple-layer cell walls, which are similar to that of the natural honeycomb (Zhang et al., 2010); moreover, they studied the influences of the microfibril angles, thickness of the cell walls, layers, shape of the cell cross-section and wood density on the elastic constants. As for the structure of grass stem (Fig. 34b), Chen and Pugno (2012b,2012c) constructed a self-similar structure (Fig. 37b) and developed a corresponding theory to investigate its linearelastic, buckling and strength properties. In particular, the study on the elastic buckling of the hierarchical structure agreed with the experimental stress–strain response very well (Chen and Pugno, 2012b).

11. Discussion and summary

With above discussions, we categorize the reviewed natural materials into four groups according to their structural features: (1) bioshells, e.g. nacre, exoskeleton of lobster or crab, armadillo and turtle shells; (2) adhesive interfaces, e.g.
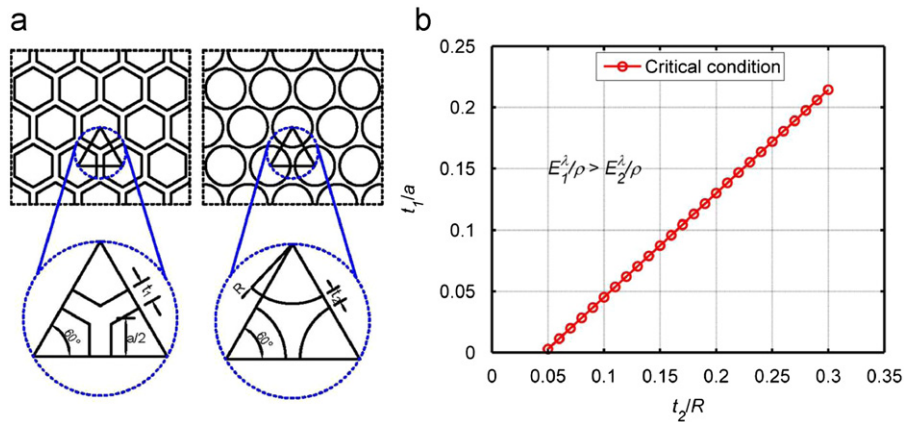
Fig. 36 – (a) Circular and hexagonal honeycomb structure; (b) efficiency between the two kinds of honeycomb.
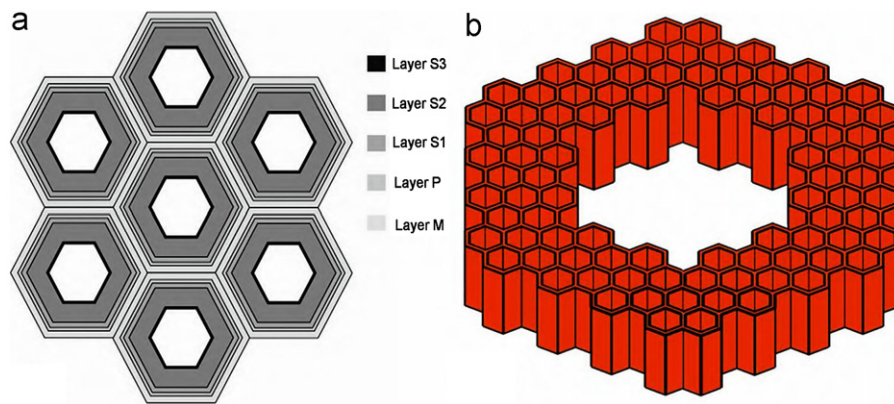
Fig. 37 – (a) Schematic of the cross-section of the hierarchical model of wood (Qing and Mishnaevsky, 2009); (b) bioinspired hierarchical structure of wood and grass stem.

gecko feet, and mussel; (3) porous materials, e.g. exoskeleton of lobster or crab, armadillo and turtle shells, diatom, and plant stem; (4) biofibres, e.g. spider silk. Despite belonging to different groups, they share some common characteristics.

In all groups except group (2), the structures themselves have a high toughness, strength and deformation ability, and the corresponding mechanisms behind them involve biomineralization, which makes biomass produce minerals to stiffen soft tissues. Addressing this problem, Aizenberg's group made a significant amount of work in order to study the biomineral and self-assembling mechanisms of the biomineralization: it is regulated by proteins and cells at the molecular level and the process is under the complex interplay of both chemical and mechanical signals (Pokroy et al., 2010). In the process, inorganic crystals nucleate first and then grow into different shapes; before these two steps, a micro-patterned amorphous precursor plays a vital role in the transformation from the amorphous to the crystalline state. For example, the amorphous precursor phase with cavity forms a porous crystal (Fratzl et al., 2010), which can be found in the armadillo and turtle shells, etc. After the crystal formation, the specialized proteins preferentially interact with certain crystal faces (Aizenberg et al., 1995), and result in a directional and bigger crystal. The principle of crystal growth is revealed based on the morphogenesis of calcitic sponge spicules—a basic skeletal element (Ilan et al., 1996).

In group (2), both cases are related to bio-adhesion between intrinsic biological structures and external substrates, and the attaching/detaching mechanisms are due to the interfacial physical, instead of chemical, bonding, such as the peeling direction, preload, structural geometry, etc. Geim et al. (2003) fabricated a gecko-tape by using the capillary and van der Waals forces, and $1\,cm^2$ patch supported $3\,N$ load, but the limitation of their material was its short durability and low detachment/attachment cycles. Recently, Wong et al. (2012) reported a strategy to synthesize self-healing (Pugno and Abdalrahman, 2011), slippery liquid infused porous surface(s) (SLIPS) with exceptional liquid- and ice-repellency, pressure stability and enhanced optical transparency by *Nepenthes*; the material shows abilities of repelling various liquids, maintaining low contact angle hysteresis, quickly restoring liquid-repellency after physical damage (within 0.1–1 s), resisting ice adhesion, functioning at high pressures and insensitive to the precise geometry of the materials; the new materials can effectively and at a low cost be used in industrial applications such as oil transportation, etc.

Besides, we also find that some of the natural materials exhibit more than one structural properties, i.e., exoskeleton of lobster or crab, armadillo and turtle shells; also, the porous structures exist in macroscopic shells and from the outer to the inner parts of the structures a porosity gradient emerges.

The forming mechanism, developed by Nature, is due to the intrinsic properties of the creatures to protect their soft parts from the predators, at the same time, it reduces the body load when they move and absorb energy when they fall from height.

Other different natural materials, such as another marine species—deep-sea sponge (Aizenberg et al., 2005)—also exhibit a hierarchical structural skeleton with more than six levels, spanning the length scale from nanometers to centimeters; the skeleton shows not only high mechanical properties but also a typical fiber-optical properties (Aizenberg et al., 2004), which are similar to commercial telecommunication fibers. In particular, the interferometric refractive-index profiling revealed that the core of the spicules with high refractive index is comparable to that of vitreous silica with the exception of an oscillating (or saw-shaped) refractive-index pattern, from the inner part surrounding the core to the outer part of the spicule within its layered structures (Sundar et al., 2003).

According to observations, the biophysical processes (e.g. biomineralization) and the different structures of natural materials can be both incorporated into the bio-inspired design or synthesis of artificial materials. Regarding the potential applications of these bio-inspired materials, they hold promising applications in designing different devices to meet emerging demands in various fields, such as engineering, physics, biology, medicine and materials science. Moreover, thanks to their designed multi-functionality, the bio-inspired materials will take an even greater role in medicine compared to other materials, for example, in the newborn field of tissue engineering, which needs bioscaffolds with simultaneously proper strength, toughness and stiffness, biocompatibility, biodegradability, and so on (Moutos et al., 2007). Specifically, Huebsch and Mooney (2009) emphasized the importance of the dynamic behavior and other variables of natural materials for medical applications; meanwhile, they point out that the integration of the chemical and physical stimuli at all hierarchical levels is necessary to create smart and multifunctional materials that can be recognized by protein or cells and used as an effective template to replace diseased targets or grow neotissues. In summary, we have discussed how Nature provides a variety of designing principles by evolving such mysterious but rich materials systems; these optimized systems are far beyond our imaginations and are more complex than our existing engineering materials. Thus, learning lessons from Nature materials is a novel and important way to create new engineering materials, e.g. spiderman suit (Pugno, 2007,2008). To the end, we collected and discussed mechanisms for several natural materials, from animals to plants, by reviewing literature and focusing on the structure–mechanical relationship. These mechanisms show that effective mechanical properties are closely related to their hierarchical structures, despite neglecting chemical elements at molecular levels, which are also very important aspects in forming the properties. The appearance of hierarchy during the evolution of biological materials (and their hyper-elastic constitutive laws) is in sharp contrast with our current design of nano-hierarchical (and mainly elastic–plastic) engineering materials, suggesting that hierarchy is the key for scaling up the fascinating intrinsic properties of the nanoscale at the macroscale, including multi-functionality (Coluci et al., 2007; Pugno et al., 2008b).

Appendix: Permissions to publish

Pemissions to publish have been granted by the following copyright holders:

Fig.1 Reprinted by permission from Macmillan Publishers Ltd. [Nature Communication] (Espinosa, H.D., Juster, A.L., Latourte, F.J., Loh, O.Y., Gregoire, D., Zavattieri, P.D., 2011. Tablet-level origin of toughening in abalone shells and translation to synthetic composite materials. Nat. Commun. 2, 173), copyright (2011).

Fig. 2 Wang, R.Z., Suo, Z., Evans, A.G., Yao, N., Aksay, I.A. Deformation mechanisms in nacre. J. Mater. Res. 16(9), 2485–2493, reproduced with permission.

Fig. 3 (a) Reprinted by permission from Macmillan Publishers Ltd. [Nature] (Smith, B.L., Schäffer, T.E., Viani, M., Thompson, J.B., Frederick, N.A., Kindt, J., Belcher, A., Stucky, G.D., Morse, D.E., Hansma, P.K., 1999. Molecular mechanistic origin of the toughenss of natural adhesives, fibres and composites. Nature 399,761–763), copyright (1999); (b); (c). Reprinted from (Li, X., 2005. Nanoscale structural and mechanical characterization of natural nanocomposites: seashells. JOM, 75, 273–299), with kind permission from Springer Science and Business Media.

Fig. 4 (a) Reprinted with permission from (Schäffer, T.E., Zanetti, C.I., Proksch, R., Fritz, M., Walters, D.A., Almqvist, N., Zaremba, C.M., Belcher, A.M., Smith, B.L., Stucky, G.D., Morse, D.E., Hansma, P.K., 1997. Does abalone nacre form by hetero-epitaxial nucleation or by growth through mineral bridges. Chem. Mater. 9, 1731–1740). Copyright (1997) American Chemical Society; (b) Reprinted from Song, F., Soh, A.K., Bai, Y.L. Structural and mechanical properties of the organic matrix layers of nacre, (Biomaterials, 24, 3623–3631), copyright (2003), with permission from Elsevier.

Fig. 5 Reprinted with permission from (Li, X., Chang, W.C., Chao, Y.J., Wang, R., Chang, M., 2004. Nanoscale structural and mechanical characterization of a natural nanocomposite material: the shell of red abalone. Nano Lett. 4, 613–617). Copyright (2004) American Chemical Society.

Fig. 6 (a) Reprinted from Kamat, S., Kessler, H., Ballarini, R., Nassirou, M., Heuer, A.H., Fracture mechanisms of the *Strombus gigas* conch shell: II-micromechanics analyses of multiple cracking and large-scale crack bridging, (Acta Mater., 52, 2395–2406), copyright (2004), with permission from Elsevier; (b) Reprinted from Cox, B.N., Marshall, D.B., Concepts for bridged cracks in fracture and fatigue, (Acta Metall. Mater., 42, 341–363), copyright (1994), with permission from Elsevier.

Fig. 7 (a) Reprinted from Ji, B., Gao, H.J., Mechanical properties of nanostructures of biological material, (J. Mech. Phys. Solids, 52, 1963–1990), copyright (2004), with permission from

Elsevier; (b) Reprinted from Bertoldi, K., Bigoni, D., Drugan, W.J., Nacre: An orthotropic and bimodular elastic material, (Compos. Sci. Technol., 68, 1363–1375), copyright (2008), with permission from Elsevier.

Fig. 8 Reprinted by permission from Macmillan Publishers Ltd. [Nature] (Autumn, K., Liang, Y.A., Tonia Hsieh, S., Zesch, W., Chan, W.P., Kenny, T. W., Fearing, R., Full, R.J., 2000. Adhesive force of a single gecko foot-hair. Nature 405, 681–684), copyright (2000).

Fig. 9 (a) Reprinted from Gao, H., Wang, X., Yao, H., Gorb, S., Arzt, E., Mechanics of hierarchical adhesion structures of geckos, (Mater. Mech., 37, 275–285), copyright (2005), with permission from Elsevier; (b) Reprinted from Prowse, M.S., Wilkinson, M., Puthoff, J.B., Mayer, G., Autumn, K. Effects of humidity on the mechanical properties of gecko setae, (Acta Mater., 7, 733–738), copyright (2011), with permission from Elsevier.

Fig. 10 Tian, Y., Pesika, N., Zeng, H., Rosenberg, K., Zhao, B., McGuiggan, P., Autumn, K., 2006. Adhesion and friction in gecko toe attachment and detachment. Proc. Natl. Acad. Sci. 103, 19320–19325, copyright (2006) National Academy of Science, U.S.A.

Fig. 12 (a)–(d) From [Harrington, M.J., Masic, A., Holten-Andersen, N.,Waite, J.H., Fratzl, P., 2010. Iron-clab fibers: a metal-based biological strategy for hard flexible coatings. Science 328, 216–220]. Reprinted with permission from AAAS; (e) Waite, J.H., Holten-Andersen, N., Jewhurst, S., Sun, C.J. Mussel adhesion: finding the tricks worth mimicking, J. Adhesion, March 2005, reprinted by permission of Taylor & Francis Ltd. (http://www.tandfonline.com/toc/gadh20/current).

Fig. 13 (a), (b) Reprinted with permission from (Zhao, H., Waite, J.H., 2006. Proteins in load bearing junctions: Histidine-rich copper binding protein of mussel byssus. Biochemistry 45, 26150–29158). Copyright (2006) American Chemical Society.

Fig. 14 Zeng, H., Hwang, D.S., Israelachvili, J.N., Waite, J.H., 2010. Strong reversible Fe^{3+}-mediated bridging between DOPA-containing protein films in water. Proc. Natl. Acad. Sci. 107, 12850–12853.

Fig. 15 Reprinted with permission from (Gosline, J.M., Guerette, P.A. Ortlepp, C.S., Savage, K.N., 1999. The mechanical design of spider silks: from fibroin sequence to mechanical function. J. Exp. Biol. 202, 3295–3303. http://jeb.biologists.org/content/202/23/3295.full.pdf)

Fig. 16 Reprinted from Du, N., Liu, X., Narayanan, J., Li, L., Lek Min Lim, M., Li, D. Design of superior spider silk: from nanostructure to mechanical properties, (Biophys. J., 91, 4528–4535), copyright (2006), with permission from Elsevier.

Fig. 17 Ackbarow, T., Chen, X., Keten, S., Buehler, M.J., 2007. Hierarchies, multiple energy barriers, and robustness govern the fracture mechanics of α-helical and β-sheet protein domains. Proc. Natl. Acad. Sci. 104, 16410–16415., copyright (2007) National Academy of Science, U.S.A.

Fig. 18 Reprinted with permission from (Du, N., Yang, Z., Liu, X, Li, Y., Xu, H., 2011. Structural origin of the strain-hardening of spider silk. Adv. Funct. Mater. 21, 772–778). Copyright (2011) John Wiley and Sons.

Fig. 19 (a) Reprinted by permission from Macmillan Publishers Ltd. [Nature Materials] (Liu, Y., Shao, Z., Vollrath, F., 2005. Relationships between supercontraction andmechanical properties of spider silk. Nat. Mater. 4, 901–905), copyright

(2005); (b) Reprinted with permission from (Yang, Y., Chen, X., Shao, Z., Zhou, P., Porter, D., Knight, D.P., Vollrath, F., 2005. Toughness of spider silk at high and low temperatures. Adv. Mater. 17, 84–88). Copyright (2005) John Wiley and Sons; (c) Reprinted with permission from (Agnarsson, I., Dhinojwala, A., Sahni, V., Blackledge, T.A., 2009. spider silk as a novel high performance biomimetic muscle driven by humidity, J. Exp. Biol. 212, 1990–1994. http://jeb.biologists.org/content/212/13/1990.full).

Fig. 20 (a) Reprinted with permission from [Zhou, H., Zhang, Y., Phys. Rev. Lett., 94, 028104, 2005. http://prl.aps.org/abstract/PRL/v94/i2/e028104]. Copyright (2005) by the American Physical Society; (b) Reprinted by permission from Macmillan Publishers Ltd: [Nature Materials] (Becker, N., Oroudjev, E., Mutz, S., Cleveland, J.P., Hansma, P.K., Hayashi, C.Y., Makarov, D.E., Hansma, H.G., 2003. Molecular nano-springs in spider capture-silk threads. Nat. Mater. 2, 278–283), copyright (2003);

Fig. 21 Reprinted with permission from (Nikolov, S., Petrov, M., Lymperakis, L., Friák, M., Sachs, S., Fabritius, H., Raabe, D., Neugebauer, J., 2010. Revealing the design principles of high-performance biological composites using Ab initio and multi-scale simulations: the example of lobster vuticle. Adv. Mater. 22, 519–526). Copyright (2010) John Wiley and Sons;

Fig. 22 (a) Reprinted from Sachs, C., Fabritius, H., Raabe, D. Experimental investigation of the elastic-plastic deformation of mineralized lobster cuticle by digital image correlation. (J. Struct. Biol. 155, 409–425), copyright (2006), with permission from Elsevier; (b) Reprinted with permission from (Fabritius, H., Sachs, C., Romano, P., Raabe, D., 2009. Influence of structural principles on the mechanics of a biological fiber-Based composite material with hierarchical organization: The exoskeleton of the lobster Homarus americanus. Adv. Mater. 21, 391–400). Copyright (2009) John Wiley and Sons.

Fig. 23 and Fig. 26 Reprinted from Chen, I.H., Kiang, J.M., Correa, V., Lopez, M.I., Chen, P.Y., McKittrick, J., Meyers, M.A. Armadillo armor: mechanical testing and micro-structural evaluation, (J. Mech. Behav. Biomed. Mater. 4, 713–722), copyright (2011), with permission from Elsevier.

Fig. 24 and Fig. 25 Reprinted from Rhee, H., Horstemeyer, M.F., Ramsay, A., A study on the structure and mechanical behavior of the Dasypus novemcinctus shell. (Mater. Sci. Eng. C, 31, 363–369), copyright (2011), with permission from Elsevier.

Fig. 27 Reprinted from Rhee, H., Horstemeyer, M.F., Hwang, Y., Lim, H., El Kadiri, H., Trim, W. A study on the structure and mechanical behavior of the Terrapene carolina carapace: a pathway to design bio-inspired synthetic composites, (Mater. Sci. Eng. C, 29, 2333–2339), copyright (2009), with permission from Elsevier.

Fig. 28 (a) Reprinted with permission from (Krauss, S., Monsonego-Ornan, E., Zelzer, E., Fratzl, P., Shahar, R., 2009. Mechanical function of a complex three-dimensional suture joining the bony elements in the shell of the red-eared slider turtle, Adv. Mater. 21, 407–412). Copyright (2009) John Wiley and Sons; (b) Reprinted from Balani, K., Patel, R.R., Keshri, A.K., Lahiri, D., Agarwal, A. Multi-scale hierarchy of Chelydra serpentina: microstructure and mechanical properties of turtle shell, (J. Mech. Behav. Biomed. Mater., 4, 1440–1451), copyright (2011), with permission from Elsevier.

Fig. 29 (a) Reprinted with permission from (Krauss, S., Monsonego-Ornan, E., Zelzer, E., Fratzl, P., Shahar, R., 2009.

Mechanical function of a complex three-dimensional suture joining the bony elements in the shell of the red-eared slider turtle. Adv. Mater. 21, 407–412). Copyright (2009) John Wiley and Sons; (b) Reprinted from Rhee, H., Horstemeyer, M.F., Hwang, Y., Lim, H., El Kadiri, H., Trim, W. A study on the structure and mechanical behavior of the *Terrapene carolina* carapace: a pathway to design bio-inspired synthetic composites. (Mater. Sci. Eng. C, 29, 2333–2339), copyright (2009), with permission from Elsevier.

Fig. 30 Reproduced from (Sumper, M., Kröger, N., 2004. Silica formation in diatoms: the function of long-chain polyamines and silaffins. J. Mater . Chem. 14, 2059–2065) with permission of The Royal Society of Chemistry.

Fig. 31 Reprinted from (Hildebrand, M., Doktycz, M.J., Allison, D.P., 2008. Application of AFM in understanding biomineral formation in diatoms. Pflugers. Arch. – Eur. J. Physiol. 456, 127–137), with kind permission from Springer Science and Business Media.

Fig. 32 (a) Reprinted with permission from © R.M. Crawford, AWI Bremerhaven, copyright (2009) Trans. Tech. Publications Inc.; (b) Reprinted with permission from (Mohedas, I., Garcia, A.P., Buehler, M.J., 2011. Nanomechanics of biologically inspired helical silica nanostructures. Proc. IMechE Part N: J. Nanoeng. and Nanosys. 224, 93–100). Copyright (2010) Institution of Mechanical Engineers; (c) and (d) Reprinted with permission from (Garcia, A., Pugno, N., Buehler, M.J., 2011b. Superductile, wavy silica nanostructures inspired by diatom algae. Adv. Eng. Mater. 13, B405–B414). Copyright (2009) John Wiley and Sons.

Fig. 33 Reprinted from (Garcia, A., Sen, D., Buehler, M.J., 2011a. Hierarchical silica nanostructures inspired by diatom algae yield superior deformability, toughness and strength, Metall. Mater. Trans. A 42, 3889–3897), with kind permission from Springer Science and Business Media.

Fig. 34 (a) Reprinted from Rafsanjani, A., Derome, D., Wittel, F.K., Carmeliet, J. Computational up-scaling of anisotropic swelling and mechanical behavior of hierarchical cellular materials. (Compos. Sci. Technol., 72, 744–751), copyright (2012), with permission from Elsevier; (b) Reprinted from Gibson, L.J. Biomechanics of cellular solids, (J. Biomech., 38, 377–399), copyright (2012), with permission from Elsevier;

Fig. 35 Reprinted from (Schulgasser, K., Witztum, A., 1997. Ann. Botany 80, 35–44), copyright (1997) with permission from Oxford University Press.

Fig. 37 (a) Reprinted from Qing, H., Mishnaevsky, L. 3D hierarchical computational model of wood as a cellular material with fibril reinforced, heterogeneous multiple layers, (Mech. Mater. 41, 1034–1049), copyright (2009), with permission from Elsevier.

R E F E R E N C E S

Ackbarow, T., Chen, X., Keten, S., Buehler, M.J., 2007. Proceedings of the National Academy of Sciences 104, 16410–16415.

Agnarsson, I., Dhinojwala, A., Sahni, V., Blackledge, T.A., 2009. Journal of Experimental Biology 212, 1990–1994.

Aizenberg, J., Hanson, J., Ilan, M., Leiserowitz, L., Koetzle, T.F., Addadi, L., Weiner, S., 1995. FASEB Journal 9, 262–268.

Aizenberg, J., Sundar, C.V., Yablon, D.A., Weaver, C.J., Chen, G., 2004. Proceedings of the National Academy of Sciences 101, 3358–3363.

Aizenberg, J., Weaver, C.J., Thanawala, S.M., Sundar, C.V., Morse, E.D., Fratzl, P., 2005. Science 309, 275–278.

Autumn, K., Peattie, A.M., 2002. Integrative and Comparative Biology 42, 1081–1090.

Autumn, K., Liang, Y.A., Tonia Hsieh, S., Zesch, W., Chan, W.P., Kenny, T.W., Fearing, R., Full, R.J., 2000. Nature 405, 681–684.

Autumn, K., Sitti, M., Liang, Y.A., Peattie, A.M., Hansen, W.R., Sponberg, S., Kenny, T.W., Fearing, R., Israelachvili, J.N., Full, R.J., 2002. Proceedings of the National Academy of Sciences 99, 12252–12256.

Autumn, K., Dittmore, A., Santos, D., Spenko, M., Cutkosky, M., 2006a. Journal of Experimental Biology 209, 3569–3579.

Autumn, K., Hsieh, S.T., Dudek, D.M., Chen, J., Chitaphan, C., Full, R.J., 2006b. Journal of Experimental Biology 209, 260–272.

Balani, K., Patel, R.R., Keshri, A.K., Lahiri, D., Agarwal, A., 2011. Journal of the Mechanical Behavior of Biomedical Materials 4, 1440–1451.

Barthelat, F., Tang, H., Zavattieri, P.D., Li, C.-M., Espinosa, H.D., 2007. Journal of the Mechanics and Physics of Solids 55, 306–337.

Becker, N., Oroudjev, E., Mutz, S., Cleveland, J.P., Hansma, P.K., Hayashi, C.Y., Makarov, D.E., Hansma, H.G., 2003. Nature Materials 2, 278–283.

Begley, M.R., Philips, N.R., Compton, B.G., Wilbrink, D.V., Ritchie, R.O., Utz, M., 2012. Journal of the Mechanics and Physics of Solids 60, 1545–1560.

Bejan, A., 2000. Shape and Structure, from Engineering to Nature. Cambridge University Press, Cambridge, UK.

Bejan, A., 2001. International Journal of Heat and Mass Transfer 44, 699–704.

Bejan, A., 2005. Journal of Experimental Biology 208, 1677–1686.

Bertoldi, K., Bigoni, D., Drugan, W.J., 2008. Composites Science and Technology 68, 1363–1375.

Bhushan, B., Jung, Y.C., 2011. Progress in Materials Science 56, 1–108.

Bosia, F., Pugno, N., Buehler, M.J., 2010. Physical Review E 82, 056103.

Bosia, F., Abdalrahman, T., Pugno, N.M., 2012. Nanoscale 4, 1200–1207.

Boutry, C., Blackledge, T.A., 2010. Journal of Experimental Biology 213, 3505–3514.

Brianza, S., Amelio, P.D., Pugno, N., Delise, M., Bignardi, C., Isaia, G., 2007. Bone 40, 1635–1642.

Buehler, M.J., Ackbarow, T., 2008. Computer Methods in Biomechanics and Biomedical Engineering 11, 595–607.

Buehler, M.J., Yao, H., Gao, H., Ji, B., 2006. Modelling and Simulation in Materials Science and Engineering 14, 799–816.

Buehler, M.J., Keten, S., Ackbarow, T., 2008. Progress in Materials Science 53, 1101–1241.

Cetinkaya, M., Xiao, S., Markert, B., Stacklies, W., Gräter, F., 2011. Biophysical Journal 100, 1298–1305.

Chen, B., Wu, P.D., Gao, H., 2008a. Proceedings of the Royal Society A 464, 1639–1652.

Chen, I.H., Kiang, J.M., Correa, V., Lopez, M.I., Chen, P.Y., McKittrick, J., Meyers, M.A., 2011. Journal of the Mechanical Behavior of Biomedical Materials 4, 713–722.

Chen, P.Y., Lin, A.Y., McKittrick, J., Meyers, M.A., 2008b. Acta Biomaterialia 4, 587–596.

Chen, P.Y., Lin, A.Y., Lin, Y.S., Seki, Y., Stokes, A.G., Peyras, J., Olevsky, E.A., Meyers, M.A., McKittrick, J., 2008c. Journal of the Mechanical Behavior of Biomedical Materials 1, 208–226.

Chen, Q., Pugno, N., 2011a. Advanced Engineering Materials 13, B377–B394.

Chen, Q., Pugno, N.M., 2011b. Composites Part B 42, 2030–2037.

Chen, Q., Pugno, N.M., 2012a. EPL 98, 16005.

Chen, Q., Pugno, N.M., 2012b. European Journal of Mechanics A—Solids 34, 120–129.

Chen, Q., Pugno, N.M., 2012c. EPL 97, 26002.

Chen, Q., Pugno, N.M., 2013. European Journal of Mechanics A—Solids 37, 248–255.

Cheng, Y.T., Rodak, D.E., Wong, C.A., Hayden, C.A., 2006. Nanotechnology 17, 1359–1362.

Clegg, W.J., Kendall, K., Alford, N.M., Button, T.W., Birchall, J.D., 1990. Nature 347, 455–457.

Colgin, M.A., Lewis, R., 1998. Protein Science 7, 667–672.

Coluci, V.R., Pugno, N., Dantas, S.O., Galvao, D.S., Jorio, A., 2007. Nanotechnology 18, 335702.

Cox, B.N., Marshall, D.B., 1994. Acta Metallurgica et Materialia 42, 341–363.

Cranford, S.W., Tarakanova, A., Pugno, N.M., Buehler, M.J., 2012. Nature 482, 72–76.

Curry, J.D., 1977. Proceedings of the Royal Society of London B 196, 443–463.

Curry, J.D., 2010. Journal of the Mechanical Behavior of Biomedical Materials 3, 357–372.

Delsanto, P.P., Condat, C.A., Pugno, N., Gliozzi, A., Griffa, M., 2008. Journal of Theoretical Biology 250, 16–24.

Delsanto, P.P., Gliozzi, A., Bruno, C., Pugno, N., Carpinteri, A., 2009. Chaos, Solitons & Fractals 41, 2782–2786.

Du, N., Liu, X., Narayanan, J., Li, L., Lek Min Lim, M., Li, D., 2006. Biophysical Journal 91, 4528–4535.

Du, N., Yang, Z., Liu, X., Li, Y., Xu, H., 2011. Advanced Functional Materials 21, 772–778.

Dugdale, D.S., 1960. Journal of the Mechanics and Physics of Solids 8, 100–104.

Emile, O., Le Floch, A., Vollrath, F., 2006. Nature 440, 621.

Espinosa, H.D., Rim, J.E., Barthelat, F., Buehler, M.J., 2009. Progress in Materials Science 54, 1059–1100.

Espinosa, H.D., Juster, A.L., Latourte, F.J., Loh, O.Y., Gregoire, D., Zavattieri, P.D., 2011. Nature Communications 2, 173.

Estrin, Y., Dyskin, A.V., Pasternak, E., 2010. Materials Science and Engineering C 31, 1189–1194.

Euler, M., 2008. Physics Education 43, 57–61.

Evans, L.S., Kahn-Jetter, Z., Marks, C., Harmoney, K.R., 2007. Journal of the Torrey Botanical Society 134, 458–467.

Fabritius, H., Sachs, C., Romano, P., Raabe, D., 2009. Advanced Materials 21, 391–400.

Foelix, R., 1996. Biology of Spiders. Oxford University Press, Oxford.

Fratzl, P., 2007. Journal of the Royal Society Interface 4, 637–642.

Fratzl, P., Fischer, F.D., Svoboda, J., Aizenberg, J., 2010. Acta Biomaterialia 6, 1001–1005.

Fraztl, P., Weinkamer, R., 2007. Progress in Materials Science 52, 1263–1334.

Gao, H., Yao, H., 2004. Proceedings of the National Academy of Sciences 101, 7851–7856.

Gao, H., Ji, B., Buehler, M.J., Yao, H., 2004. Mechanics and Chemistry of Biosystems 1, 37–52.

Gao, H., Wang, X., Yao, H., Gorb, S., Arzt, E., 2005. Materials of Mechanics 37, 275–285.

Gao, H., Ji, B., Jäger, I.L., Arzt, E., Fratzl, P., 2003. Proceedings of the National Academy of Sciences 100, 5597–5600.

Garcia, A., Sen, D., Buehler, M.J., 2011a. Metallurgical and Materials Transactions A 42, 3889–3897.

Garcia, A., Pugno, N., Buehler, M.J., 2011b. Advanced Engineering Materials 13, B405–B414.

Gebeshuber, I.C., Stachelberger, H., Ganji, B.A., Fu, D.C., Yunas, J., Majlis, B.Y., 2009. Advanced Materials Research 74, 265–268.

Geim, A.K., Dubonos, S.V., Grigorieva, I.V., Novoselov, K.S., Zhukov, A.A., Shapoval, S.Y., 2003. Nature Materials 2, 461–463.

Gibson, L.J., 2005. Journal of Biomechanics 38, 377–399.

Gibson, L.J., Ashby, M.F., 1997. Cellular Solids: Structure and Properties, 2nd ed. Cambridge University Press, Cambridge, UK.

Giesa, T., Arslan, M., Pugno, N.M., Buehler, M.J., 2011. Nano Letters 11, 5038–5046.

Giesa, T., Pugno, N.M., Buehler, M.J., 2012. Physical Review E 86, 041902.

Gilbert, S.F., Loredo, G.A., Brukman, A., Burke, A.C., 2001. Evolutionary and Development 3, 47–58.

Gosline, J.M., Guerette, P.A., Ortlepp, C.S., Savage, K.N., 1999. Journal of Experimental Biology 202, 3295–3303.

Gong, B., Chen, Q., Wang, D., 2012. Materials Letters 67, 165–168.

Guiot, C., Delsanto, P.P., Carpinteri, A., Pugno, N., Mansury, Y., Deisboeck, T.S., 2006. Journal of Theoretical Biology 240, 459–463.

Guiot, C., Pugno, N., Delsanto, P.P., Deisboeck ,T.S., 2007. Physical Biology 4, P1-P6.

Hamm, C.E., Merkel, R., Springer, O., Jurkojc, P., Maier, C., Prechtel, K., Smetacek, V., 2003. Nature 421, 841–843.

Hansen, W.R., Autumn, K., 2005. Proceedings of the National Academy of Sciences 102, 385–389.

Harrington, M.J., Masic, A., Holten-Andersen, N., Waite, J.H., Fratzl, P., 2010. Science 328, 216–220.

Hayashi, C.Y., Lewis, R., 1998. Journal of Molecular Biology 275, 773–784.

Hildebrand, M., York, E., Kelz, J.I., Davis, A.K., Frigeri, L.G., Allison, D.P., Doktycz, M.J., 2006. Journal of Materials Research 21, 2689–2698.

Hildebrand, M., Doktycz, M.J., Allison, D.P., 2008. Pflügers Archiv European Journal of Physiology 456, 127–137.

Hildebrand, M., Holton, G., Joy, D.C., Doktycz, M.J., Allison, D.P., 2009. Journal of Microscopy 235, 172–187.

Hofstetter, K., Gamstedt, E.K., 2008. Holzforschung 63, 130–138.

Holten-Andersen, N., Mates, T.E., Toprak, M.S., Stucky, G.D., Zok, F.W., Waite, J.H., 2009. Langmuir 25, 3323–3326.

Holten-Andersen, N., Harrington, M.J., Birkedal, H., Lee, B.P., Messersmith, P.B., Lee, K.Y., Waite, J.H., 2011. Proceedings of the National Academy of Sciences 108, 2651–2655.

Huber, G., Mantz, H., Spolenak, R., Mecke, K., Jacobs, K., Gorb, S.N., Arzt, E., 2005. Proceedings of the National Academy of Sciences 102, 16293–16296.

Huemmerich, D., Scheibel, T., Vollrath, F, Cohen, S., Gat, U., Ittah, S., 2004. Current Biology 14, 2070–2074.

Huebsch, N., Mooney, D.J., 2009. Nature 462, 426–432.

Hwang, D.S., Zeng, H., Masic, A., Harrington, M.J., Israelachvili, J.N., Waite, J.H., 2010. Journal of Biological Chemistry 285, 25850–25858.

Ilan, M., Aizenberg, J., Gilor, O., 1996. Proceedings of the Royal Society of London B 263, 133–139.

Jackson, A.P., Vincent, J.F.V., 1989. Composite Science and Engineering 36, 255–266.

Jackson, A.P., Vincent, J.F.V., Turner, R.M., 1988. Proceedings of the Royal Society of London B 234, 415–440.

Jäger, I., Fratzl, P., 2000. Biophysical Journal 79, 1737–1746.

Jagota, A., Hui, C.-Y., 2011. Materials Science and Engineering R 72, 253–292.

Ji, B., 2008. Journal of Biomechanics 41, 259–266.

Ji, B., Gao, H.J., 2004. Journal of the Mechanics and Physics of Solids 52, 1963–1990.

Kamat, S., Su, X., Ballarini, R., Heuer, A.H., 2000. Nature 405, 1036–1040.

Kamat, S., Kessler, H., Ballarini, R., Nassirou, M., Heuer, A.H., 2004. Acta Materialia 52, 2395–2406.

Kaplan, D.L., 1998. Current Opinion in Solid State & Materials Science 3, 232–236.

Karam, G.N., Gibson, L.J., 1994. Materials Science and Engineering C 2, 113–132.

Karam, G.N., Gibson, L.J., 1995a. International Journal of Solids and Structures 32, 1259–1283.

Karam, G.N., Gibson, L.J., 1995b. International Journal of Solids and Structures 32, 1284–1306.

Kelly, S.P., Sensenig, A., Lorentz, K.A., Blackledge, T.A., 2011. Zoology 114, 233–238.

Keten, S., Buehler, M.J., 2008. Physical Review Letters 100, 198301.

Keten, S., Buehler, M.J., 2010. Journal of the Royal Society Interface 7, 1709–1721.

Keten, S., Xu, Z., Ihle, B., Buehler, M.J., 2010. Nature Materials 9, 359–367.

Krauss, S., Monsonego-Ornan, E., Zelzer, E., Fratzl, P., Shahar, R., 2009. Advanced Materials 21, 407–412.

Kuraku, S., Usuda, R., Kuratani, S., 2005. Evolution and Development 7, 3–17.

Lakes, R., 1993. Nature 361, 511–515.

Launey, M.E., Ritchie, R.O., 2009. Advanced Materials 21, 2103–2110.

Lee, H., Lee, B.P., Messersmith, P.B., 2007. Nature 448, 338–341.

Lepore, E., Pugno, N., 2011. BioNanoscience 1, 136–143.

Lepore, E., Antoniolli, F., Buono, M., Brianza, S., Carpinteri, A., Pugno, N., 2008. Journal of Nanomaterials 194, 524–528.

Lepore, E., Pugno, F., Pugno, N.M., 2012a. J. Adhesion 88, 820–830.

Lepore, E., Marchioro, A., Isaia, M., Buehler, M.J., Pugno, N., 2012b. PLoS ONE 7, e30500.

Li, X., 2007. Journal of the Minerals Metals & Materials Society 59, 71–74.

Li, X., Chang, W.C., Chao, Y.J., Wang, R., Chang, M., 2004. Nano Letters 4, 613–617.

Lin, A.Y.M., Meyers, M.A., 2009. Journal of the Mechanical Behavior of Biomedical Materials 2, 607–612.

Lin, A.Y.M., Meyers, M.A., Vecchio, K.S., 2006. Materials Science and Engineering C 26, 1380–1389.

Lin, Q., Gourdon, D., Sun, C.J., Holten-Andersen, N., Anderson, T.H., Waite, J.H., Israelachvili, J.N., 2007. Proceedings of the National Academy of Sciences 104, 3782–3786.

Liu, Y., Shao, Z., Vollrath, F., 2005. Nature Materials 4, 901–905.

Lin, Q., Gourdon, D., Sun, C., Holten Andersen, N., Anderson, T.H., Herbert-Waite, J., Israelachvili, J.N., 2007. Proceedings of the National Academy Science 104, 3782–3786.

Losic, D., Pillar, R.J., Dilger, T., Mitchell, J.G., Voelcker, N.H., 2007. Journal of Porous Materials 14, 61–69.

Meyers, M.A., Chen, P.Y., Lin, A.Y.M., Seki, Y., 2008a. Progress in Materials Science 53, 1–206.

Meyers, M.A., Lin, A.Y.M., Chen, P.Y., Muyco, J., 2008b. Journal of the Mechanical Behavior of Biomedical Materials 1, 76–85.

Mita, K., Ichimura, S., James, T., 1994. Journal of Molecular Evolution 38, 583–592.

Mohedas, I., Garcia, A.P., Buehler, M.J., 2011. Proceedings of the IMechE Part N: Journal of Nanoengineering and Nanosystems 224, 93–100.

Moutos, F.T., Freed, L.E., Guilak, F., 2007. Nature Materials 6, 162–167.

Niklas, K.J., 1997a. Annals of Botany 80, 275–287.

Niklas, K.J., 1997b. Annals of Botany 80, 437–448.

Niklas, K.J., 1998. Annals of Botany 81, 11–21.

Nikolov, S., Petrov, M., Lymperakis, L., Friák, M., Sachs, S., Fabritius, H., Raabe, D., Neugebauer, J., 2010. Advanced Materials 22, 519–526.

Nova, A., Keten, S., Pugno, N., Redaelli, A., Buehler, M.J., 2010. Nano Letters 10, 2626–2634.

Pantano, A., Pugno, N., Gorb, S., 2011. International Journal of Fracture 171, 169–175.

Papka, S.D., Kyriakides, S., 1994. Journal of the Mechanics and Physics of Solids 42, 1499–1532.

Papka, S.D., Kyriakides, S., 1998a. International Journal of Solids and Structures 35, 239–267.

Papka, S.D., Kyriakides, S., 1998b. Acta Materialia 46, 2765–2776.

Pérez-Rigueiro, P., Elices, M., Plaza, G., Real, J.I., Guinea, G.V., 2005. Journal of Experimental Biology 208, 2633–2639.

Persson, B.N.J., 2003. Journal of Chemical Physics 118, 7614–7621.

Persson, B.N.J., Gorb, S., 2003. Journal of Chemical Physics 119, 11437–11444.

Pokroy, B., Aichmayer, B., Schenk, A.S., Haimov, B., Kang, S.H., Fratzl, P., Aizenberg, J., 2010. Journal of the American Chemical Society 132, 14355–14357.

Porter, D., Vollrath, F., Shao, Z., 2005. European Physics Journal E 16, 199–206.

Prowse, M.S., Wilkinson, M., Puthoff, J.B., Mayer, G., Autumn, K., 2011. Acta Materialia 7, 733–738.

Pugno, N., 2007. Journal of Physics: Condensed Matter 19, 395001.

Pugno, N., 2008. Nano Today 3, 35–41.

Pugno, N., 2010. Materials Today 13, 40–43.

Pugno, N., 2011. International Journal of Fracture 171, 185–193.

Pugno, N., Abdalrahman, T., 2011. International Space Elevator Consortium, CLIMB 1, 77–84.

Pugno, N., Lepore, E., 2008a. Journal of Adhesion 89, 949–962.

Pugno, N., Lepore, E., 2008b. Biosystem 94, 218–222.

Pugno, N., Carpinteri, A., Delsanto., P.P., Bosia, F., Gliozzi, A., 2008a. Physical Review E 78, 046103–1/5.

Pugno, N., Bosia, F., Carpinteri, A., 2008b. Small 4, 1044–1052.

Pugno, N., Lepore, E., Toscano, S., Pugno, F., 2011. J. Adhesion 87, 1059–1072.

Pugno, N., Bosia, F., Abdalrahman, T., 2012. Physical Review E 85, 011903.

Pugno, N.M., 2006. Nanotechnology 17, 5480–5484.

Qin, Z., Buehler, M.J., 2011. ACS Nano 5, 3034–3042.

Qin, Z., Kreplak, L., Buehler, M.J., 2009. PLoS ONE 4, e7294.

Qin, Z., Buehler, M.J., 2012. Applied Physics Letters 101, 083702.

Qing, H., Mishnaevsky, L., 2009. Mechanics of Materials 41, 1034–1049.

Raabe, D., Sachs, C., Romano, P., 2005a. Acta Materialia 53, 4281–4292.

Raabe, D., Romano, P., Sachs, C., Al-Sawalmih, A., Brokmeier, H.-G., Yi, S.-B., Servos, G., Hartwig, H.G., 2005b. Journal of Crystal Growth 283, 1–7.

Raabe, D., Romano, P., Sachs, C., Fabritius, H., Al-Sawalmih, A., Yi, S.-B., Servos, G., Hartwig, H.G., 2006. Materials Science and Engineering A 421, 143–153.

Raabe, D., Al-Sawalmih, A., Yi, S.B., Fabritius, H., 2007. Acta Biomaterials 3, 882–895.

Rafsanjani, A., Derome, D., Wittel, F.K., Carmeliet, J., 2012. Composites Science and Technology 72, 744–751.

Rhee, H., Horstemeyer, M.F., Hwang, Y., Lim, H., El Kadiri, H., Trim, W., 2009. Materials Science and Engineering C 29, 2333–2339.

Rhee, H., Horstemeyer, M.F., Ramsay, A., 2011. Materials Science and Engineering C 31, 363–369.

Rieppel, O., 2009. Science 325, 154–155.

Rim, J.E., Zavattieri, P., Juster, A., Espinosa, H.D., 2011. Journal of the Mechanical Behavior of Biomedical 4, 190–211.

Ritchie, R.O., 1988. Materials Science and Engineering A 103, 15–28.

Ritchie, R.O., Buehler, M.J., Hansma, P., 2009. Physics Today 62, 41–47.

Romano, P., Fabritius, H., Raabe, D., 2007. Acta Biomaterials 3, 301–309.

Rousseau, M., Lopez, E., Couté, A., Mascarel, G., Smith, D.C., Naslain, R., Bourrat, X., 2005. Journal of Structural Biology 149, 149–157.

Rousseau, M., Meibom, A., Gèze, M., Bourrat, X., Angellier, M., Lopez, E., 2009. Journal of Structural Biology 165, 190–195.

Russell, A.P., 1975. Journal of Zoology London 176, 437–476.

Sachs, C., Fabritius, H., Raabe, D., 2006a. Journal of Structural Biology 155, 409–425.

Sachs, C., Fabritius, H., Raabe, D., 2006b. Journal of Materials Research 21, 1987–1995.

Sachs, C., Fabritius, H., Raabe, D., 2008. Journal of Structural Biology 161, 120–132.

Savage, K.N., Gosline, J.M., 2008. Journal of Experimental Biology 211, 1948–1957.

Schäffer, T.E., Zanetti, C.I., Proksch, R., Fritz, M., Walters, D.A., Almqvist, N., Zaremba, C.M., Belcher, A.M., Smith, B.L., Stucky, G.D., Morse, D.E., Hansma, P.K., 1997. Chemistry of Materials 9, 1731–1740.

Schulgasser, K., Witztum, A., 1997. Annals of Botany 80, 35–44.

Sen, D., Buehler, M.J., 2011. Science Reports 35, 1.

Sen, D., Garcia, A., Buehler, M.J., 2011. Journal of Nanomechanics and Micromechanics 1, 112–118.

Shafiq, Z., Cui, J., Pastor-Pérez, L., San Miguel, V., Gropeanu, R.A., Serrano, C., del Campo, A., 2012. Angewandte Chemie 124, 4408–4411.

Smith, B.L., Schäffer, T.E., Viani, M., Thompson, J.B., Frederick, N.A., Kindt, J., Belcher, A., Stucky, G.D., Morse, D.E., Hansma, P.K., 1999. Nature 399, 761–763.

Song, F., Soh, A.K., Bai, Y.L., 2003. Biomaterials 24, 3623–3631.

Srinivasan, A.V., Haritos, G.K., Hedberg, F.L., 1991. Applied Mechanics Reviews 44, 463–481.

Stempflé, P.H., Pantalé, O., 2007. Nanotechnology 4, 712–729.

Stempflé, P.H., Pantalé, O., Rousseau, M., Lopez, E., Bourrat, X., 2010. Materials Science and Engineering C 30, 715–721.

Sumper, M., Kröger, N., 2004. Journal of Materials Chemistry 14, 2059–2065.

Sundar, C.V., Yablon, D.A., Grazul, L.J., Ilan, M., Aizenberg, J., 2003. Nature 424, 899–900.

Tang, H., Barthelat, F., Espinosa, H.D., 2007. Journal of the Mechanics and Physics of Solids 55, 1410–1538.

Tang, H., Buehler, M.J., Moran, B., 2009. Annals of Biomedical Engineering 37, 1117–1130.

Tesson, B., Hildebrand, M., 2010. Journal of Structural Biology 169, 62–74.

Thompson, D.W., 1945. On Growth and Form. Cambridge University Press, New York (pp. 789–804).

Tian, Y., Pesika, N., Zeng, H., Rosenberg, K., Zhao, B., McGuiggan, P., Autumn, K., 2006. Proceedings of the National Academy of Sciences 103, 19320–19325.

Truman, R., 2008. Southern Medical Journal 101, 581–582.

Truman, R.W., Kumaresan, J.A., Mcdonough, C.M., Job, C.K., Hastings, R.C., 1991. Epidemiology and Infection 106, 549–560.

Valle, L.D., Nardi, A., Toni, M., Emera, D., Alibardi, L., 2009. Journal of Anatomy 214, 284–300.

Varenberg, M., Pugno, N., Gorb, S., 2010. Soft Matter 6, 3269–3272.

Venner, S., Casas, Jérôme, 2005. Proceedings of the Royal Society B 272, 1587–1592.

Vickaryous, M.K., Hall, B.K., 2006. Journal of Morphology 267, 1273–1283.

Vollrath, F., 2000. Reviews in Molecular Biotechnology 74, 67–83.

Waite, J.H., Holten-Andersen, N., Jewhurst, S., Sun, C.J., 2005. Journal of Adhesion 81, 297–317.

Wang, R.Z., Suo, Z., Evans, A.G., Yao, N., Aksay, I.A., 2001. Journal of Materials Research 16, 2485–2493.

Weaver, J.C., Aizenberg, J., Fantner, G.E., Kisailus, D., Woesz, A., Allen, P., Fields, K., Porter, M.J., Zok, F.W., Hansma, P.K., Fratzl, P., Morse, D.E., 2007. Journal of Structural Biology 158, 93–106.

Wegst, U.G.K., Ashby, M.F., 2004. Philosophical Magazine 84, 2167–2181.

Wegst, U.G.K., Ashby, M.F., 2007. Journal of Materials Science 42, 9005–9014.

West, G.B., Brown, J.H., Enquist, B.J., 1997. Science 276, 122–126.

Wilbrink, D.V., Utz, M., Ritchie, R.O., Begley, M.R., 2010. Applied Physics Letters 97, 193701.

Wong, T.-S., Kang, S.H., Tang, S.K.Y., Smythe, E.J., Hatton, B.D., Grinthal, A., Aizenberg, J., 2012. Nature 477, 443–447.

Work, R.W., 1977. Textile Research Journal 47, 650–662.

Xu, Z.-H., Li, X., 2011. Advanced Functional Materials 21, 3883–3888.

Yang, Y., Chen, X., Shao, Z., Zhou, P., Porter, D., Knight, D.P., Vollrath, F., 2005. Advanced Materials 17, 84–88.

Yao, H., Gao, H., 2006. Journal of the Mechanics and Physics of Solids 54, 1120–1146.

Zeng, H., Hwang, D.S., Israelachvili, J.N., Waite, J.H., 2010. Proceedings of the National Academy of Sciences 107, 12850–12853.

Zhang, K., Duan, H.L., Karihaloo, B.L., Wang, J., 2010. Proceedings of the National Academy of Sciences 107, 9502–9506.

Zhao, H., Waite, J.H., 2006. Biochemistry 45, 26150–29158.

Zhou, H., Zhang, Y., 2005. Physical Review Letters 94, 028104.